J Fourier Anal Appl (2018) 24:719–758
https://doi.org/10.1007/s00041-017-9536-8

Phase Retrieval with One or Two Diffraction Patterns by Alternating Projections with the Null Initialization

Pengwen Chen[1] · **Albert Fannjiang**[2] · **Gi-Ren Liu**[2]

Received: 29 July 2016 / Revised: 24 February 2017 / Published online: 20 March 2017

Abstract Alternating projection (AP) of various forms, including the parallel AP (PAP), real-constrained AP (RAP) and the serial AP (SAP), are proposed to solve phase retrieval with at most two coded diffraction patterns. The proofs of geometric convergence are given with sharp bounds on the rates of convergence in terms of a spectral gap condition. To compensate for the local nature of convergence, the null initialization is proposed to produce good-quality initial guess. Numerical experiments show that the null initialization is more accurate than the spectral initialization and that AP converges faster to the true object than other iterative schemes such as the Wirtinger flow (WF). In numerical experiments AP with the null initialization converges globally to the true object.

Keywords Phase retrieval · Alternating projections · Local convergence · Spectral gap · Null initialization

Mathematics Subject Classification 42B · 65T · 90C

1 Introduction

With wide-ranging applications in science and technology, phase retrieval has recently attracted a flurry of activities in the mathematics community (see a recent review

Communicated by Peter G. Casazza.

✉ Albert Fannjiang
fannjiang@math.ucdavis.edu

[1] Department of Applied Mathematics, National Chung Hsing University, Taichung 402, Taiwan

[2] Department of Mathematics, University of California, Davis, CA 95616, USA

[53] and references therein). Chief among these applications is the coherent X-ray diffractive imaging of a single particle using a coherent, high-intensity source such as synchrotrons and free-electron lasers.

In the so-called *diffract-before-destruct* approach, the structural information of the sample particle is captured by an ultra-short and ultra-bright X-ray pulse and recorded by a CCD camera [16,17,54]. To this end, reducing the radiation exposure and damage is crucial. Due to the high frequency of the illumination field, the recorded data are the intensity of the diffracted field whose phase needs to be recovered by mathematical and algorithmic techniques. This gives rise to the problem of phase retrieval with non-crystalline structures.

The earliest algorithm of phase retrieval for a non-periodic object (such as a single molecule) is the Gerchberg–Saxton algorithm [33] and its variant, error reduction [31]. The basic idea is alternating projection (AP), going all the way back to the works of von Neumann, Kaczmarz and Cimmino in the 1930s [21,37,55]. And these further trace the history back to Schwarz [52] who in 1870 used AP to solve the Dirichlet problem on a region given as a union of regions each having a simple to solve Dirichlet problem.

For any vector y let $|y|$ be the vector such that $|y|[j] = |y[j]|, \forall j$. In a nutshell, phase retrieval is to solve the equation of the form $b = |A^* x_0|$ where $x_0 \in \mathcal{X} \subseteq \mathbb{C}^n$ represents the unknown object, $A^* \in \mathbb{C}^{N\times n}$ the diffraction/propagation process and $b^2 \in \mathbb{R}^N$ the diffraction pattern(s). The subset $\mathcal{X}$ represents all prior constraints on the object. Also, the number of data N is typically greater than the number n of components in x_0.

Phase retrieval can be formulated as the following feasibility problem

$$\text{Find} \quad \hat{y} \in A^*\mathcal{X} \cap \mathcal{Y}, \quad \mathcal{Y} := \{y \in \mathbb{C}^N : |y| = b\}. \tag{1}$$

From $\hat{y}$ the object is estimated via pseudo-inverse

$$\hat{x} = (A^*)^\dagger \hat{y}. \tag{2}$$

Let P_1 be the projection onto $A^*\mathcal{X}$ and P_2 the projection onto $\mathcal{Y}$ defined as

$$P_2 z = b \odot \frac{z}{|z|}, \quad z \in \mathbb{C}^N$$

where $\odot$ denotes the Hadamard product and $z/|z|$ the componentwise division. Where z vanishes, $z/|z|$ is chosen to be 1 by convention. Then AP is simply the iteration of the composite map

$$P_1 P_2 y \tag{3}$$

starting with an initial guess $y^{(1)} = A^* x^{(1)}, x^{(1)} \in \mathcal{X}$.

The main structural difference between AP in the classical setting [21,37,55] and the current setting is the *non-convexity* of the set $\mathcal{Y}$, rendering the latter much more

difficult to analyze. Moreover, AP for phase retrieval is well known to have stagnation problems in practice, resulting in poor reconstruction [31,32,43].

In our view, numerical stagnation has more to do with the measurement scheme than non-convexity: the existence of multiple solutions when only one (uncoded) diffraction pattern is measured even if additional positivity constraint is imposed on the object. However, if the diffraction pattern is measured with a random mask (a coded diffraction pattern), then the uniqueness of solution under the real-valuedness constraint is restored with probability one [28]. In addition, if two independently coded diffraction patterns are measured, then the uniqueness of solution, up to a global phase factor, holds almost surely without any additional prior constraint [28] (see Proposition 1.1).

The main goal of the present work is to show by analysis and numerics that under the uniqueness framework for phase retrieval with coded diffraction patterns of [28], AP has a significantly sized basin of attraction at x_0 and that this basin of attraction can be reached by an effective initialization scheme, called the null initialization. In practice, numerical stagnation of AP disappears under the uniqueness measurement schemes of [28].

Specifically, our goal is two-fold: (i) prove the local convergence of various versions of AP under the uniqueness framework of [28] (Theorems 5.7, 6.3 and 7.3) and (ii) propose a novel method of initialization, the null initialization, that compensates for the local nature of convergence and results in global convergence in practice. In practice AP with the null initialization converges globally to the true object.

1.1 Set-up

Let us recall the measurement schemes of [28].

Let $x_0(\mathbf{n})$, $\mathbf{n} = (n_1, n_2, \ldots, n_d) \in \mathbb{Z}^d$, be a discrete object function supported in

$$\mathcal{M} = \{0 \le m_1 \le M_1, 0 \le m_2 \le M_2, \ldots, 0 \le m_d \le M_d\}.$$

We assume $d \ge 2$.

Define the d-dimensional *discrete-space Fourier transform* of x_0 as

$$\sum_{\mathbf{n}\in\mathcal{M}} x_0(\mathbf{n}) e^{-i2\pi \mathbf{n}\cdot\mathbf{w}}, \quad \mathbf{w} = (w_1, \ldots, w_d) \in [0,1]^d. \tag{4}$$

However, only the *intensities* of the Fourier transform, called the diffraction pattern, are measured

$$\sum_{\mathbf{n}=-\mathbf{M}}^{\mathbf{M}} \sum_{\mathbf{m}\in\mathcal{M}} x_0(\mathbf{m}+\mathbf{n})\overline{x_0(\mathbf{m})} e^{-i2\pi \mathbf{n}\cdot\mathbf{w}}, \quad \mathbf{M} = (M_1, \ldots, M_d)$$

which is the Fourier transform of the autocorrelation

$$R(\mathbf{n}) = \sum_{\mathbf{m}\in\mathcal{M}} x_0(\mathbf{m}+\mathbf{n})\overline{x_0(\mathbf{m})}.$$

Here and below the over-line means complex conjugacy.

Note that R is defined on the enlarged grid

$$\widetilde{\mathcal{M}} = \{(m_1,\dots,m_d)\in\mathbb{Z}^d : -M_1 \le m_1 \le M_1, \cdots, -M_d \le m_d \le M_d\}$$

whose cardinality is roughly 2^d times that of $\mathcal{M}$. Hence by sampling the diffraction pattern on the grid

$$\mathcal{L} = \left\{(w_1,\dots,w_d) \mid w_j = 0, \frac{1}{2M_j+1}, \frac{2}{2M_j+1}, \dots, \frac{2M_j}{2M_j+1}\right\}$$

we can recover the autocorrelation function by the inverse Fourier transform. This is the *standard oversampling* with which the diffraction pattern and the autocorrelation function become equivalent via the Fourier transform [44,45].

A coded diffraction pattern is measured with a mask whose effect is multiplicative and results in a *masked object* of the form $\tilde{x}_0(\mathbf{n}) = x_0(\mathbf{n})\mu(\mathbf{n})$ where $\{\mu(\mathbf{n})\}$ is an array of random variables representing the mask. In other words, a coded diffraction pattern is just the plain diffraction pattern of a masked object.

We will focus on the effect of *random phases* $\phi(\mathbf{n})$ in the mask function $\mu(\mathbf{n}) = |\mu|(\mathbf{n})e^{i\phi(\mathbf{n})}$ where $\phi(\mathbf{n})$ are independent, continuous real-valued random variables and $|\mu|(\mathbf{n}) \neq 0, \forall \mathbf{n}\in\mathcal{M}$ (i.e. the mask is transparent).

For simplicity we assume $|\mu|(\mathbf{n}) = 1, \forall \mathbf{n}$ which gives rise to a *phase* mask and an *isometric* propagation matrix

$$(1-\text{mask}) \quad A^* = c\Phi\ \text{diag}\{\mu\}, \tag{5}$$

i.e. $AA^* = I$ (with a proper choice of the normalizing constant c), where Φ is the *oversampled* d-dimensional discrete Fourier transform (DFT). Specifically $\Phi \in \mathbb{C}^{|\tilde{\mathcal{M}}|\times|\mathcal{M}|}$ is the sub-column matrix of the standard DFT on the extended grid $\tilde{\mathcal{M}}$ where $|\mathcal{M}|$ is the cardinality of $\mathcal{M}$.

If the non-vanishing mask μ does not have a uniform transparency, i.e. $|\mu|(\mathbf{n}) \neq 1, \forall \mathbf{n}$, then we can define a new object vector $|\mu|\odot x_0$ and a new isometric propagation matrix

$$A^* = c\Phi\ \text{diag}\left\{\frac{\mu}{|\mu|}\right\}$$

with which to recover the new object first.

When two phase masks μ_1, μ_2 are deployed, the propagation matrix A^* is the stacked coded DFTs, i.e.

$$\text{(2-mask case)} \quad A^* = c \begin{bmatrix} \Phi \ \mathrm{diag}\{\mu_1\} \\ \Phi \ \mathrm{diag}\{\mu_2\} \end{bmatrix}. \tag{6}$$

With proper normalization, A^* is isometric.

We convert the d-dimensional ($d \geq 2$) grid into an ordered set of index. Let $n = |\mathcal{M}|$ and N the total number of measured data. In other words, $A \in \mathbb{C}^{N \times n}$.

Let $\mathcal{X}$ be a nonempty closed convex set in $\mathbb{C}^n$ and let

$$[x]_{\mathcal{X}} = \arg\min_{x' \in \mathcal{X}} \|x' - x\| \tag{7}$$

denote the projection onto $\mathcal{X}$.

Phase retrieval is to find a solution x to the equation

$$b = |A^* x|, \quad x \in \mathcal{X}. \tag{8}$$

We focus on the following two cases.

(i) *One-pattern case* A^* is given by (5), $\mathcal{X} = \mathbb{R}^n$ or $\mathbb{R}^n_+$.
(ii) *Two-pattern case* A^* is given by (6), $\mathcal{X} = \mathbb{C}^n$ (i.e. $[x]_{\mathcal{X}} = x$).

For the two-pattern case, AP for the formulation (1) shall be called the parallel AP (PAP) as the rows of A^* and the diffraction data are treated equally and simultaneously, in contrast to the serial AP (SAP) which splits the diffraction data into two blocks according to the masks and treated alternately.

As the vectorized version of the original object supported in $\mathcal{M} \subset \mathbb{Z}^d$, x_0 is a *line object* if the convex hull of the original object support in $\mathbb{R}^d$ is a line segment.

Now we recall the uniqueness theorem of phase retrieval with coded diffraction patterns.

Proposition 1.1 [28] (Uniqueness of Fourier phase retrieval) *Suppose that x_0 is not a line object and that x is a solution of the phase retrieval problem (8) for either the one-pattern or two-pattern case. Then $x = e^{i\theta} x_0$ for some constant $\theta \in \mathbb{R}$ with probability one.*

Remark 1.2 The main improvement over the classical uniqueness theorem [36] is that while the classical result works with generic (thus random) objects Proposition 1.1 deals with a given deterministic object. By definition, deterministic objects belong to the measure zero set excluded in the classical setting of [36]. It is crucial to endow the probability measure on the ensemble of random masks, which we can manipulate, instead of the space of unknown objects, which we cannot control.

The proof of Proposition 1.1 is given in [28] where more general uniqueness theorems can be found. Proposition 1.1 is the basis of the measurement schemes

studied in the present work and can further be used to identify any fixed point x_* of AP with the true solution if the norm condition $\|x_0\| = \|b\|$ is satisfied (Remark 4.3).

Phase retrieval solution is unique only up to a constant of modulus one no matter how many coded diffraction patterns are measured. Thus a reasonable error metric for an estimate $\hat{x}$ of the true solution x_0 is given by

$$\min_{\theta\in\mathbb{R}} \|e^{i\theta}\hat{x} - x_0\|. \tag{9}$$

Our framework and methods can be extended to more general, non-isometric measurement matrix A^* as follows. Let $A^* = QR$ be the QR-decomposition of A^* where Q is isometric and R is upper-triangular. Indeed,

$$Q = A^*(AA^*)^{-1/2} \tag{10}$$

if A (and hence R) is full-rank. Now we can define a new object vector Rx and a new isometric measurement matrix Q with which to recover Rx first.

1.2 Comparison with Other Work in Literature

Much of recent mathematical literature on phase retrieval focuses on generic frames and random measurements, see e.g. [1–5,11,12,22,24,27,35,42,47,50,53,53,56,57,59]. Among the mathematical works on Fourier phase retrieval e.g. [7,13–15,18,26,28–30,36,38,39,43,46,49,51,58], only a few focus on analysis and development of efficient algorithms.

Despite the theoretical appeal of a convex minimization approach to phase retrieval [12,14,15], the tremendous increase in dimension results in impractically slow computation for large problems. Recently, new non-convex approaches become popular again because of their computational efficiency among other benefits [13,46,47].

One purpose of the present work is to compare these newer approaches with AP, arguably the simplest of all non-convex approaches. An important difference of the measurement schemes in these papers from ours is that their coded diffraction patterns are *not* oversampled. In this connection, we emphasize that reducing the number of coded diffraction patterns is crucial for the diffract-before-destruct approach and it is better to oversample than to increase the number of coded diffraction patterns. Another difference is that these newer iterative schemes such as the Wirtinger flow (WF) [13] are not of the projective type. In Sect. 8, we provide a detailed numerical comparison between AP of various forms and WF.

More important, to compensate for the local nature of convergence we develop a novel procedure, the null initialization, for finding a sufficiently close initial guess. The null initialization is significantly different from the spectral initialization proposed in [11,13,47]. In Sect. 2.4 we give a theoretical comparison and in Sect. 8 a numerical comparison between these initialization methods. We will see that the initialization with the null initialization is more accurate than with the spectral ini-

tialization and AP with the null initialization converges faster and produces more accurate results than the Fourier-domain Douglas–Rachford algorithm studied in [18].

As pointed out above, there are more than one way of formulating phase retrieval, especially with two (or more) diffraction patterns, as a feasibility problem. While PAP is analogous to Cimmino's approach to AP [21], SAP is closer in spirit to Kaczmarz's [37]. SAP converges significantly faster than PAP but produces less accurate results in the presence of measurement noise (Sect. 8). In Sects. 5 and 7 we prove that both schemes are locally convergent to the true solution with bounds on rates of convergence. For phase retrieval with a Gaussian random measurement, local convergence for PAP was proved in [47,56]. SAP with Fourier measurements were tested numerically in [29,58] but its convergence was not proved.

Among the vast literature on AP, we mention only the most relevant literature and refer the reader to the reviews [6,25] for a more complete list of references. Von Neumann's convergence theorem [55] for AP with two closed subspaces is extended to the setting of closed convex sets in [10,20] and, starting with [33], the application of AP to the non-convex setting of phase retrieval has been extensively studied [7,8, 31,32,43].

In [41] local convergence theorems were developed for AP for non-convex problems. However, the technical challenge in applying the theory in [41] to phase retrieval lies precisely in formulating the precise conditions of the measurement schemes and verifying the main assumption of linear regular intersection therein.

In contrast, in the present work, what guarantees the geometric convergence and gives an often sharp bound on the convergence rate (as demonstrated in Fig 7) is the spectral gap condition which can be readily verified under the uniqueness framework of [28] (see Propositions 5.4 and 6.1 below).

Reference [49] (Corollary 12) asserts the existence of a local basin of attraction of the feasible set (1) which includes AP in the one-pattern case and PAP in the two-pattern case (but not SAP). From this and the uniqueness theorem (Proposition 1.1) convergence to the true solution, up to a global phase factor, follows (i.e. a singleton with an arbitrary global phase factor). However, Corollary 12 of [49] asserts a *sublinear* power-law convergence with an unspecified power. In contrast, we prove a linear convergence and give a spectral gap bound on the convergence rate for various versions of AP, including SAP which is emphatically not covered by [49].

Indeed, as further elaborated in Sect. 9, general purpose theorems for AP *without* regard to the design of measurement schemes can only guarantee a sub-optimal sense of convergence.

The paper proceeds as follows. In Sect. 2, we discuss the null initialization versus the spectral initialization. In Sect. 3, we formulate AP of various forms and in Sect. 4 we discuss the limit points and the fixed points of AP. We prove local convergence to the true solution for the PAP in Sect. 5 and for the real-constraint AP in Sect. 6. In Sect. 7 we prove local convergence for the SAP. In Sect. 8, we present numerical experiments and compare our approach with the Wirtinger flow and its truncated version [11,13]. In Sect. 9, we discuss the pros and cons of our results and point out the open problems to be further studied.

2 The Null Initialization

For a nonconvex minimization problem such as phase retrieval, the accuracy of the initialization as the estimate of the object has a great impact on the performance of any iterative schemes.

The following observation motivates our approach to effective initialization. Let I be a subset of $\{1, \dots, N\}$ and I_c its complement such that $b[i] \le b[j]$ for all $i \in I$, $j \in I_c$. In other words, $\{b[i] : i \in I\}$ are the "weaker" signals and $\{b[j] : j \in I_c\}$ the "stronger" signals. Let $|I|$ be the cardinality of the set I. Then $\{a_i\}_{i\in I}$, the columns of A, are nearly orthogonal to x_0 if $|I|/N$ is sufficiently small (see Sect. 2.4). This suggests the following constrained least squares solution

$$x_{\text{null}} \in \arg\min \left\{ \sum_{i\in I} |a_i^* x|^2 : x \in \mathcal{X}, \|x\| = \|x_0\| \right\}$$

may be a reasonable initialization. Note that x_{null} is not uniquely defined as αx_{null}, with $|\alpha| = 1$, is also a null vector. Moreover, there may be more than one linearly independent null vectors.

We pause to emphasize that the constraint $\|x_{\text{null}}\| = \|x_0\|$ is introduced for ease of comparison and is completely irrelevant when used in conjunction with AP since the AP map $\mathcal{F}$ (see (32) below for definition) is scaling-invariant in the sense that $\mathcal{F}(cx) = \mathcal{F}(x)$, for any $c > 0$. Also, in many imaging problems, the norm of the true object, like the constant phase factor, is either recoverable by other prior information or irrelevant to the quality of reconstruction.

Denote the sub-column matrices consisting of $\{a_i\}_{i\in I}$ and $\{a_j\}_{j\in I_c}$ by A_I and A_{I_c}, respectively.

Define a dual vector x_{dual} as

$$x_{\text{dual}} \in \arg\max \left\{ \|A_{I_c}^* x\|^2 : x \in \mathcal{X}, \|x\| = \|x_0\| \right\}. \tag{11}$$

Like x_{null}, x_{dual} is not uniquely defined.

2.1 Isometric A^*

For isometric A^*, select any

$$x_{\text{null}} \in \arg\min \left\{ \sum_{i\in I} |a_i^* x|^2 : x \in \mathcal{X}, \|x\| = \|b\| \right\}. \tag{12}$$

Since for an isometric A^*

$$\|A_I^* x\|^2 + \|A_{I_c}^* x\|^2 = \|x\|^2,$$

we have

$$\{x_{\text{null}}\} = \{x_{\text{dual}}\}, \tag{13}$$

i.e. the set of null vectors is the same as the set of dual vectors. Eqs. (13) and (12) can be used to construct a null vector from $A_{I_c}A_{I_c}^*$ by the power method.

Let $\mathbf{1}_c$ be the characteristic function of the complementary index I_c with $|I_c| = \gamma N$. The default choice for γ is the median value $\gamma = 0.5$. Below x_{rand} denote random initialization whose pixels are given by, e.g. independent uniform random variables over $[0, 1]$.

Algorithm 1: The null initialization

Random initialization: $x_1 = x_{\text{rand}}$
Loop:
for $k = 1 : k_{\max} - 1$ **do**
  $x_k' \leftarrow A(\mathbf{1}_c \odot A^* x_k)$;
  $x_{k+1} \leftarrow [x_k']_{\mathcal{X}} / \|[x_k']_{\mathcal{X}}\|$
end
Output: $\hat{x}_{\text{dual}} = x_{k_{\max}} \|x_0\| / \|x_{\text{rand}}\|$.

In the case of nonunique x_{dual}, the output of Algorithm 1 will depend on the (random) initialization x_{rand}. As shown in Sect. 8, the null initialization is remarkably accurate (Figs. 2 and 4) and stable with respect to measurement noise (Fig. 9).

2.2 Non-isometric A^*

When A^* is non-isometric such as the standard Gaussian random matrix (see below), the power method is still applicable with the following modification.

For a full rank A, let $A^* = QR$ be the QR-decomposition of A^* where Q is isometric and R is a full-rank, upper-triangular square matrix. Let $z = Rx$, $z_0 = Rx_0$ and $z_{\text{null}} = Rx_{\text{null}}$ in Eq. (8). Clearly, z_{null} is a null vector for the isometric phase retrieval problem $b = |Qz|$ in the sense of (12).

Let I and I_c be the index sets as above. Let

$$\hat{z} \in \arg\max_{\|z\|=1} \|Q_{I_c} z\|. \tag{14}$$

Then

$$x_{\text{null}} = \beta R^{-1} \hat{z}$$

where

$$\beta = \frac{\|x_0\|}{\|R^{-1}\hat{z}\|}$$

may be an unknown parameter in the non-isometric case. As pointed out above, when x_{null} with an arbitrary parameter β is used as initialization in conjunction with AP, the first iteration of AP would recover the true value of β as AP is totally independent of any real constant factor.

2.3 The Spectral Initialization

Here we compare the null initialization with the spectral initialization used in [13] and the truncated spectral initialization used in [11].

Algorithm 2: The spectral initialization

1 **Random initialization:** $x_1 = x_{\text{rand}}$
2 **Loop:**
3 **for** $k = 1 : k_{\max} - 1$ **do**
4 $\quad x_k' \leftarrow A(|b|^2 \odot A^* x_k)$;
5 $\quad x_{k+1} \leftarrow [x_k']_{\mathcal{X}} / \|[x_k']_{\mathcal{X}}\|$;
6 **end**
7 **Output:** $x_{\text{spec}} = x_{k_{\max}} \|x_0\| / \|x_{\text{rand}}\|$.

The key difference between Algorithms 1 and 2 is the different weights used in step 4 where the null initialization uses $\mathbf{1}_c$ and the spectral vector method uses $|b|^2$ (Algorithm 2). The truncated spectral initialization uses a still different weighting

$$x_{\text{t-spec}} = \arg\max_{\|x\|=1} \|A\left(\mathbf{1}_\tau \odot |b|^2 \odot A^* x\right)\| \tag{15}$$

where $\mathbf{1}_\tau$ is the characteristic function of the set

$$\{i : |A^* x[i]| \le \tau \|b\|\}$$

with an adjustable parameter τ. Both γ of Algorithm 1 and τ of (15) can be optimized by tracking and minimizing the residual $\|b - |A^* x_k|\|$.

As shown in the numerical experiments in Sect. 8 (Figs. 2 and 4), the choice of weight significantly affects the quality of initialization, with the null initialization as the best performer (cf. Sect. 2.4).

Moreover, because the null initialization depends only on the choice of the index set I and not explicitly on the variation in the components of b, the method is noise-tolerant and performs well with noisy data (Fig. 9).

2.4 Error Bound

As in [11,13] we assume for the rigorous error bound that the measurement matrix is given by the complex Gaussian case $A = \Re(A) + i\Im(A)$, where the entries of

$\Re(A), \Im(A)$ are i.i.d. standard normal random variables. The following error bound is in terms of the closely related error metric

$$\|x_0 x_0^* - x_{\text{null}} x_{\text{null}}^*\|^2 = 2\|x_0\|^4 - 2|x_0^* x_{\text{null}}|^2 \tag{16}$$

which has the advantage of being independent of the global phase factor.

According to [19], for

$$n < |I| \ll N \ll |I|^2 \tag{17}$$

we have the error bound

$$\|x_0 x_0^* - x_{\text{null}} x_{\text{null}}^*\|^2 \le c_0 \|x_0\|^4 |I|/N \tag{18}$$

with probability at least

$$1 - c_1 \exp\left(-c_2 |I|^2/N\right)$$

where the constants c_1, c_2 are independent of the parameters in (17). Namely, the right hand side of (18) can be made arbitrarily small with probability close to 1.

In comparison, the performance guarantees for the spectral initialization in [47], [13] (Theorem 3.3) and [11] (Proposition 3) deal with a *fixed* level of relative error, independent of N.

We mention by passing that the initialization by the resampling techniques ([47] and [13], Theorem 5.1) requires in practice a large number of coded diffraction patterns and does not apply to the present set-up.

3 Alternating Projections

First we introduce some notation and convention that are frequently used in the subsequent analysis.

The vector space $\mathbb{C}^n = \mathbb{R}^n \oplus_{\mathbb{R}} i\mathbb{R}^n$ is isomorphic to $\mathbb{R}^{2n}$ via the map

$$G(v) := \begin{bmatrix} \Re(v) \\ \Im(v) \end{bmatrix}, \quad \forall v \in \mathbb{C}^n \tag{19}$$

and endowed with the real inner product

$$\langle u, v \rangle := \Re(u^* v) = G(u)^\top G(v), \quad u, v \in \mathbb{C}^n. \tag{20}$$

We say that u and v are (real-)orthogonal to each other (denoted by $u \perp v$) iff $\langle u, v \rangle = 0$. The same isomorphism exists between $\mathbb{C}^N$ and $\mathbb{R}^{2N}$.

Let $y \odot y'$ and y/y' be the component-wise multiplication and division between two vectors y, y', respectively. For any $y \in \mathbb{C}^N$ define the phase vector $\omega \in \mathbb{C}^N$ with $\omega[j] = y[j]/|y[j]|$ where $|y[j]| \neq 0$. When $|y[j]| = 0$ the phase can be assigned any

value in $[0, 2\pi]$. For simplicity, we set the default value $y[j]/|y[j]| = 1$ whenever the denominator vanishes.

It is important to note that for the measurement schemes (5) and (6), the mask function by assumption is an array of independent, continuous random variables. Hence the components of $y_0 = A^*x_0$ are continuous random variables. Therefore $b = |y_0|$ almost surely vanishes nowhere. However, we will develop the AP method without this assumption and without specifically appealing to the structure of the measurement schemes (5) and (6) unless stated otherwise.

Let A^* be any $N \times n$ matrix, $b = |A^*x_0|$ and

$$F(x) = \frac{1}{2}\||A^*x| - b\|^2 = \frac{1}{2}\|A^*x\|^2 - \sum_{j\in J} b[j]|a_j^*x| + \frac{1}{2}\|b\|^2 \tag{21}$$

where

$$J := \{j : b[j] > 0\}.$$

As noted above, for our measurement schemes (5) and (6), $J = \{1, 2, \ldots, N\}$ almost surely.

In view of (21), the only possible hinderance to differentiability over the reals for F is the sum-over-J term. Indeed, we have the following result.

Proposition 3.1 *The function $F(x)$ is infinitely differentiable in the real and imaginary parts of x in the open set*

$$\{x \in \mathbb{C}^n : |a_j^*x| > 0, \quad \forall j \in J\}. \tag{22}$$

In particular, for an isometric A^*, $F(x)$ is infinitely differentiable in the neighborhood of x_0 defined by

$$\|x_0 - x\| < \min_{j\in J} b[j]. \tag{23}$$

Proof Observe that

$$|a_j^*x| = |a_j^*x_0 - a_j^*(x_0 - x)| \geq b[j] - |a_j^*(x_0 - x)| \geq b[j] - \|x - x_0\|,$$

and hence $|a_j^*x| > 0$ if $\|x_0 - x\| < b[j]$. The proof is complete. □

Consider the smooth function

$$f(x, u) = \frac{1}{2}\|A^*x - u \odot b\|^2 = \frac{1}{2}\|A^*x\|^2 - \sum_{j\in J} \Re(x^*a_j b[j]u[j]) + \frac{1}{2}\|b\|^2 \tag{24}$$

where $x \in \mathbb{C}^n$ and

$$u \in U := \{(u[i]) \in \mathbb{C}^N : |u[i]| = 1, \ \forall i\}. \tag{25}$$

We can write

$$F(x) = \min_{u \in U} f(x, u) \tag{26}$$

which has many minimizers if $x^* a_j b[j] = 0$ for some j. Since

$$\nabla_u f\left(x, \frac{A^* x}{|A^* x|}\right) = 0 \tag{27}$$

we select by convention the minimizer $u = A^* x/|A^* x|$ where again $u[j] = 1$ if $a_j^* x = 0$. Define the complex gradient

$$\nabla_x f(x, u) := \frac{\partial f(x, u)}{\partial \Re(x)} + i \frac{\partial f(x, u)}{\partial \Im(x)} = AA^* x - A(u \odot b) \tag{28}$$

and consider the alternating minimization procedure

$$u^{(k)} = \arg\min_{u \in U} f(x^{(k)}, u), \tag{29}$$

$$x^{(k+1)} = \arg\min_{x \in \mathcal{X}} f(x, u^{(k)}) \tag{30}$$

each of which is a (constrained) least squares problem.

By (27) and (28), the minimizer (30) is given by

$$x^{(k+1)} = (A^*)^\dagger (u^{(k)} \odot b), \quad u^{(k)} = \frac{A^* x^{(k)}}{|A^* x^{(k)}|} \tag{31}$$

where the pseudo-inverse

$$(A^*)^\dagger = (AA^*)^{-1} A$$

of A^* becomes A if A^* isometric which we assume henceforth.

Eq. (31) can be written as the fixed point iteration

$$x^{(k+1)} = \mathcal{F}(x^{(k)}), \quad \mathcal{F}(x) = \left[A\left(b \odot \frac{A^* x}{|A^* x|}\right)\right]_{\mathcal{X}}. \tag{32}$$

In the one-pattern case, (32) is exactly Fienup's Error Reduction algorithm [31].

The AP map (32) can be formulated as the projected gradient method [34,40]. In the small neighborhood of x_0 where $F(x)$ is smooth (Proposition 3.1), we have

$$\nabla F(x) = \nabla_x f(x, u) = AA^* x - A(b \odot u), \quad \text{with } u = \frac{A^* x}{|A^* x|} \tag{33}$$

and hence

$$\mathcal{F}(x) = [x - \nabla F(x)]_{\mathcal{X}}\,. \tag{34}$$

The object domain formulation (32) is equivalent to the Fourier domain formulation (3) by the change of variables $y = A^*x$ and letting

$$P_1 y = A^*[Ay]_{\mathcal{X}}, \quad P_2 y = b \odot \frac{y}{|y|}.$$

where $F(x)$ is not differentiable, the right hand side of (33) is an element of the subdifferential of F. Therefore, the AP map (32) can be viewed as the generalization of the projected gradient method to the non-smooth setting.

We shall study the following three versions of AP. The first is the PAP

$$\mathcal{F}(x) = A\left(b \odot \frac{A^*x}{|A^*x|}\right) \tag{35}$$

to be applied to the two-pattern case. The second is the real-constrained AP (RAP)

$$\mathcal{F}(x) = \left[A\left(b \odot \frac{A^*x}{|A^*x|}\right)\right]_{\mathcal{X}}, \quad \mathcal{X} = \mathbb{R}^n,\ \mathbb{R}^n_+ \tag{36}$$

to be applied to the one-pattern case.

The third is the SAP defined as follows. Following [29] in the spirit of Kaczmarz, we partition the measurement matrix and the data vector into parts and treat them sequentially.

Let $A_l^*, b_l, l = 1, 2$, be the individual masked measurement matrices and data, respectively. We can write

$$A^* = \begin{bmatrix} \frac{1}{\sqrt{2}} A_1^* \\ \frac{1}{\sqrt{2}} A_2^* \end{bmatrix}, \quad b = \begin{bmatrix} \frac{1}{\sqrt{2}} b_1 \\ \frac{1}{\sqrt{2}} b_2 \end{bmatrix} \quad \text{with} \quad b_l = |A_l^* x_0|, \quad l = 1, 2,$$

where $A_l^*, l = 1, 2$, are isometric.

Let $y \in \mathbb{C}^N$ be written as $y = [y_1^\top, y_2^\top]^\top$. Instead of (1), we now formulate the phase retrieval problem as the following feasibility problem

$$\text{Find} \quad \hat{y} \in \cap_{l=1}^2 \left(A_l^* \mathcal{X} \cap \mathcal{Y}_l\right), \quad \mathcal{Y}_l := \{y_l : |y_l| = b_l\}. \tag{37}$$

As the projection onto the non-convex set $A_l^* \mathcal{X} \cap \mathcal{Y}_l$ is not explicitly known, we use the approximation instead

$$\mathcal{F}_l(x) = A_l\left(b_l \odot \frac{A_l^* x}{|A_l^* x|}\right), \quad l = 1, 2, \tag{38}$$

and consider the SAP map

$$\mathcal{F}(x) = \mathcal{F}_2(\mathcal{F}_1(x)). \tag{39}$$

In contrast, the PAP map (35)

$$\mathcal{F}(x) = A\left(b \odot \frac{A^*x}{|A^*x|}\right) = \frac{1}{2}(\mathcal{F}_1(x) + \mathcal{F}_2(x)) \tag{40}$$

is the arithmetic average of $\mathcal{F}_1$ and $\mathcal{F}_2$. By Proposition 1.1, x_0 is the only fixed point of both $\mathcal{F}_1$ and $\mathcal{F}_2$ (see Sect. 4 for definition).

4 Fixed Points

We study the fixed points of PAP and RAP.

Following [29] we consider the the generalized AP (PAP) map

$$\mathcal{F}_\sigma(x) := \left[A\left(b \odot \sigma \odot \frac{A^*x}{|A^*x|}\right)\right]_{\mathcal{X}}, \quad \mathcal{X} = \mathbb{C}^n \text{ or } \mathbb{R}^n \text{ or } \mathbb{R}^n_+ \tag{41}$$

where

$$\sigma \in U, \quad \sigma[j] = 1, \quad \text{if } a_j^* x_* \neq 0. \tag{42}$$

We call x_* a **fixed point** of AP if there exists

$$\sigma \in U = \{u = (u[i]) \in \mathbb{C}^N : |u[i]| = 1, \ \forall i\}$$

satisfying (42) such that the fixed point equation

$$x_* = \mathcal{F}_\sigma(x_*) \tag{43}$$

holds [29]. In other words, the definition (43) allows flexibility of phase where A^*x_* vanishes.

The following result identifies any limit point of the AP iterates with a fixed point of AP.

Proposition 4.1 *The AP iterates $x^{(k)} = \mathcal{F}^k(x^{(1)})$ with any starting point $x^{(1)}$, where $\mathcal{F}$ is given by (35) or (36), is bounded and every limit point is a fixed point of AP in the sense (42)–(43).*

Proof Due to (26) , (29) and (30),

$$\begin{aligned} 0 \le F(x^{(k+1)}) &= f(x^{(k+1)}, u^{(k+1)}) \le f(x^{(k+1)}, u^{(k)}) \le f(x^{(k)}, u^{(k)}) \\ &= F(x^{(k)}), \quad \forall k, \end{aligned} \tag{44}$$

and hence AP yields a non-increasing sequence $\{F(x^{(k)})\}_{k=1}^{\infty}$.

For an isometric A^*,

$$\nabla_x f(x,u) = x - A(u \odot b),$$

and

$$\mathcal{F}(x) = [x - \nabla_x f(x,u)]_{\mathcal{X}}, \quad u = \frac{A^* x}{|A^* x|}.$$

implying

$$x^{(k+1)} = \left[x^{(k)} - \nabla_x f(x^{(k)}, u^{(k)})\right]_{\mathcal{X}}. \tag{45}$$

Now by the convex projection theorem (Proposition B.11 of [9]).

$$\left\langle x^{(k)} - \nabla_x f(x^{(k)}, u^{(k)}) - x^{(k+1)}, x - x^{(k+1)} \right\rangle \le 0, \quad \forall x \in \mathcal{X} \tag{46}$$

Setting $x = x^{(k)}$ in Eq. (46) we have

$$\left\| x^{(k)} - x^{(k+1)} \right\|^2 \le \left\langle \nabla_x f(x^{(k)}, u^{(k)}), x^{(k)} - x^{(k+1)} \right\rangle. \tag{47}$$

Furthermore, the descent lemma (Proposition A.24 of [9]) yields

$$f(x^{(k+1)}, u^{(k)}) \le f(x^{(k)}, u^{(k)}) + \left\langle x^{(k+1)} - x^{(k)}, \nabla_x f(x^{(k)}, u^{(k)}) \right\rangle + \frac{1}{2} \left\| x^{(k+1)} - x^{(k)} \right\|^2. \tag{48}$$

From Eq. (44), Eqs. (48) and (47), we have

$$\begin{aligned} F(x^{(k)}) - F(x^{(k+1)}) &\ge f(x^{(k)}, u^{(k)}) - f(x^{(k+1)}, u^{(k)}) \\ &\ge \langle x^{(k)} - x^{(k+1)}, \nabla_x f(x^{(k)}, u^{(k)}) \rangle - \frac{1}{2} \left\| x^{(k+1)} - x^{(k)} \right\|^2 \\ &\ge \frac{1}{2} \left\| x^{(k+1)} - x^{(k)} \right\|^2. \end{aligned} \tag{49}$$

As a nonnegative and non-increasing sequence, $\{F(x^{(k)})\}_{k=1}^{\infty}$ converges and then (49) implies

$$\lim_{k \to \infty} \left\| x^{(k+1)} - x^{(k)} \right\| = 0. \tag{50}$$

By the definition of $x^{(k)}$ and the isometry of A^*, we have

$$\left\| x^{(k)} \right\| \le \left\| A(b \odot u^{(k-1)}) \right\| \le \|b\|,$$

and hence $\{x^{(k)}\}$ is bounded. Let $\{x^{(k_j)}\}_{j=1}^{\infty}$ be a convergent subsequence and x_* its limit. Eq. (50) implies that

$$\lim_{j\to\infty} x^{(k_j+1)} = x_*.$$

If A^*x_* vanishes nowhere, then $\mathcal{F}$ is continuous at x_*. Passing to the limit in $\mathcal{F}(x^{(k_j)}) = x^{(k_j+1)}$ we get $\mathcal{F}(x_*) = x_*$. Namely, x_* is a fixed point of $\mathcal{F}$.

Suppose $a_l^* x_* = 0$ for some l. By the compactness of the unit circle and further selecting a subsequence from the previous subsequence, still denoted by $\{x^{(k_j)}\}$, we have

$$\lim_{j\to\infty} \frac{A^*x^{(k_j)}}{|A^*x^{(k_j)}|} = \frac{A^*x_*}{|A^*x_*|} \odot \sigma \tag{51}$$

for some $\sigma \in U$ satisfying (42) which is to account for the difference in the limit on the left hand side and $a_l^* x_*/|a_l^* x_*| = 1$ on the right (by our convention). Now passing to the limit in $\mathcal{F}(x^{(k_j)}) = x^{(k_j+1)}$ we have

$$x_* = \mathcal{F}_u(x_*)$$

implying that x_* is a fixed point of AP. □

Since the true object is unknown, the following norm criterion is useful for distinguishing the phase retrieval solutions from the non-solutions among many coexisting fixed points.

Proposition 4.2 *Let $\mathcal{F}$ be the AP map (32) with isometric A^*. If a fixed point x_* of AP in the sense (42)–(43) satisfies $\|x_*\| = \|b\|$, then x_* is a phase retrieval solution almost surely. On the other hand, if x_* is not a phase retrieval solution, then $\|x_*\| < \|b\|$.*

Remark 4.3 If the isometric A^* is specifically given by (6) or (5), then by Propositions 4.2 and 1.1 we can identify any fixed point x_* with the unique phase retrieval solution x_0, if the norm condition $\|x_*\| = \|b\|$ is satisfied.

Proof By the convex projection theorem (Proposition B.11 of [9])

$$\|[v]_{\mathcal{X}}\| \le \|v\|, \quad \forall v \in \mathbb{C}^n \tag{52}$$

where the equality holds if and only if $v \in \mathcal{X}$. Hence

$$\begin{aligned} \|x_*\| &= \left\| \left[A\left(\frac{A^*x_*}{|A^*x_*|} \odot b \odot u \right) \right]_{\mathcal{X}} \right\| \\ &\le \left\| A\left(\frac{A^*x_*}{|A^*x_*|} \odot b \odot u \right) \right\| \\ &\le \left\| \frac{A^*x_*}{|A^*x_*|} \odot b \odot u \right\| = \|b\|. \end{aligned} \tag{53}$$

Clearly $\|x_*\| = \|b\|$ holds if and only if both inequalities in Eq. (53) are equalities. The second inequality is an equality only when

$$\frac{A^*x_*}{|A^*x_*|} \odot b \odot u = A^*z \quad \text{for some} z \in \mathbb{C}^n. \tag{54}$$

By Eqs. (52) and (54) the first inequality in Eq. (53) becomes an equality only when $z \in \mathcal{X}$.

Since $AA^* = I$ the fixed point equation (43) implies $z = x_*$ and

$$\frac{A^*x_*}{|A^*x_*|} \odot b \odot u = A^*x_*.$$

Thus $b = |A^*x_*|$. □

5 Parallel AP

Define

$$B_x = A \operatorname{diag}\left[\frac{A^*x}{|A^*x|}\right] \tag{55}$$

$$\mathcal{B}_x = \begin{bmatrix} \Re(B_x) \\ \Im(B_x) \end{bmatrix}. \tag{56}$$

When $x = x_0$, we will drop the subscript x and write simply B and $\mathcal{B}$.

Whenever $F(x)$ is twice-differentiable at x, we have as before

$$\begin{aligned} \nabla F(x) &= \frac{\partial F(x)}{\partial \Re(x)} + i\frac{\partial F(x)}{\partial \Im(x)} \\ &= A(A^*x - b \odot u), \quad u = \frac{A^*x}{|A^*x|} \end{aligned} \tag{57}$$

and

$$\begin{aligned} \nabla^2 F(x)\zeta &:= \nabla\langle \nabla F(x), \zeta\rangle \\ &= \frac{\partial\langle \nabla F(x), \zeta\rangle}{\partial \Re(x)} + i\frac{\partial\langle \nabla F(x), \zeta\rangle}{\partial \Im(x)}, \quad \forall \zeta \in \mathbb{C}^n. \end{aligned} \tag{58}$$

Recall from (20) that $\langle u, v\rangle := \Re(u^*v)$.

Proposition 5.1 *Suppose $|a_j^*x| > 0$ for all $j \in J = \{i : b[i] > 0\}$ (i.e. $F(x)$ is smooth at x by Proposition 3.1). For all $\zeta \in \mathbb{C}^n$, we have*

$$\langle \nabla F(x), \zeta\rangle = \Re(x^*\zeta) - b^\top \Re(B_x^*\zeta), \tag{59}$$

and

$$\begin{aligned}\left\langle \zeta, \nabla^2 F(x)\zeta \right\rangle &= \|\zeta\|^2 - \left\langle \Im\left(B_x^*\zeta\right), \rho_x \odot \Im\left(B_x^*\zeta\right)\right\rangle \\ &= \|\zeta\|^2 - \left\langle \mathcal{B}_x^\top G(-i\zeta), \rho_x \odot \mathcal{B}_x^\top G(-i\zeta)\right\rangle \end{aligned} \tag{60}$$

with

$$\rho_x[j] = \lim_{\epsilon\to 0^+} \frac{b[j]}{\epsilon + |a_j^* x|}, \quad j = 1, \ldots, N.$$

Proof Rewriting (21) as

$$F(x) = \frac{1}{2}\|A^* x\|^2 - \sum_{j\in J} f_j(x) + \frac{1}{2}\|b\|^2, \quad f_j(x) := b[j]|a_j^* x|, \tag{61}$$

we analyze the derivative of each term on the right hand side of (61).

Since $AA^* = I$, the gradient and the Hessian of $\|A^* x\|^2/2$ are x and I, respectively.

For f_j, we have Taylor's expansion in real and imaginary parts of x in the complex form

$$f_j(x + \epsilon\zeta) = f_j(x) + \epsilon\langle \nabla f_j(x), \zeta\rangle + \frac{\epsilon^2}{2}\left\langle \zeta, \nabla^2 f_j(x)\zeta\right\rangle + O(\epsilon^3) \tag{62}$$

where

$$\langle \nabla f_j(x), \zeta\rangle = \frac{b[j]}{|a_j^* x|}\left\langle a_j^* x, a_j^*\zeta\right\rangle, \quad j \in J \tag{63}$$

and

$$\left\langle \zeta, \nabla^2 f_j(x)\zeta\right\rangle = \frac{b[j]}{|a_j^* x|}\left|\frac{\Re(a_j^* x)}{|a_j^* x|}\Im(a_j^*\zeta) - \frac{\Im(a_j^* x)}{|a_j^* x|}\Re(a_j^*\zeta)\right|^2, \quad j \in J. \tag{64}$$

Observe that

$$\left\langle \frac{a_j^* x}{|a_j^* x|}, a_j^*\zeta\right\rangle = \Re(B_x^*\zeta)[j], \quad j \in J$$

and

$$\frac{\Re(a_j^* x)}{|a_j^* x|}\Im(a_j^*\zeta) - \frac{\Im(a_j^* x)}{|a_j^* x|}\Re(a_j^*\zeta) = \Im(B_x^*\zeta)[j] = \mathcal{B}_x^\top G(-i\zeta)[j], \quad j \in J$$

which, together with (62) and (64), yield the desired results (59) and (60). □

Next we investigate the conditions under which $\nabla^2 F(x_0)$ is positive definite.

5.1 Spectral Gap

Let $\lambda_1 \geq \lambda_2 \geq \cdots \geq \lambda_{2n} \geq \lambda_{2n+1} = \cdots = \lambda_N = 0$ be the singular values of $\mathcal{B}$ with the corresponding right singular vectors $\{\eta_k \in \mathbb{R}^N\}_{k=1}^N$ and left singular vectors $\{\xi_k \in \mathbb{R}^{2n}\}_{k=1}^{2n}$.

Proposition 5.2 *We have* $\lambda_1 = 1, \lambda_{2n} = 0$, $\eta_1 = |A^* x_0|$ *and*

$$\xi_1 = G(x_0) = \begin{bmatrix} \Re(x_0) \\ \Im(x_0) \end{bmatrix}, \quad \xi_{2n} = G(-ix_0) = \begin{bmatrix} \Im(x_0) \\ -\Re(x_0) \end{bmatrix}$$

Proof Since

$$B^* x = \Omega^* A^* x, \quad \Omega = \operatorname{diag}\left[\frac{A^* x_0}{|A^* x_0|}\right]$$

we have

$$\Re[B^* x_0] = \mathcal{B}^\top \xi_1 = |A^* x_0|, \quad \Im[B^* x_0] = \mathcal{B}^\top \xi_{2n} = 0 \tag{65}$$

and hence the results. □

Proposition 5.3

$$\begin{aligned} \lambda_2 &= \max\{\|\Im[B^* u]\| : u \in \mathbb{C}^n, iu \perp x_0, \|u\| = 1\} \\ &= \max\{\|\mathcal{B}^\top u\| : u \in \mathbb{R}^{2n}, u \perp \xi_1, \|u\| = 1\}. \end{aligned} \tag{66}$$

Proof Note that

$$\Im[B^* u] = \mathcal{B}^\top G(-iu).$$

The orthogonality condition $iu \perp x_0$ is equivalent to

$$G(x_0) \perp G(-iu).$$

Hence, by Proposition 5.2, ξ_2 is the maximizer of the right hand side of (66), yielding the desired value λ_2. □

We recall the spectral gap property that is a key to local convergence of the one-pattern and the two-pattern case.

Proposition 5.4 [18] *Suppose* $x_0 \in \mathbb{C}^n$ *is not a line object. For* A^* *given by* (5) *or* (6) *with independently and continuously distributed mask phases, we have* $\lambda_2 < 1$ *with probability one.*

Remark 5.5 We emphasize that Proposition 5.4 does not assume any object constraint besides the assumption of non-line object even in the one-pattern case (5).

Proposition 5.6 *Let*

$$\lambda_2(x) = \max\{\|\Im(B_x^* u)\| : u \in \mathbb{C}^n, \langle u, ix\rangle = 0, \|u\| = 1\}. \tag{67}$$

Let γ be a convex combination of x and x_0 with $\langle x_0, x\rangle > 0$. Then

$$\left\|\Im(B_\gamma^*(x - x_0))\right\| = \left\|\mathcal{B}_\gamma^\top G(-i(x - x_0))\right\| \le \lambda_2(\gamma)\|x - x_0\|. \tag{68}$$

Proof Since $\langle x_0, x\rangle > 0$,

$$c_1 := \|\gamma\|^{-2}\langle \gamma, x_0\rangle > 0, \quad c_2 := \|\gamma\|^{-2}\langle \gamma, x\rangle > 0 \tag{69}$$

and we can write the orthogonal decomposition

$$x_0 = c_1\gamma + \gamma_1, \quad x = c_2\gamma + \gamma_2 \tag{70}$$

with some vectors γ_1, γ_2 satisfying $\langle \gamma_1, \gamma\rangle = \langle \gamma_2, \gamma\rangle = 0$.

By (55),

$$\Im(B_\gamma^*\gamma) = \Im(|A^*\gamma|) = 0$$

and hence

$$\Im(B_\gamma^*(x - x_0)) = \Im(B_\gamma^*(\gamma_2 - \gamma_1))$$

from which it follows that

$$\|x - x_0\|^{-1}\|\Im(B_\gamma^*(x - x_0))\| \le \|\gamma_2 - \gamma_1\|^{-1}\|\Im(B_\gamma^*(\gamma_2 - \gamma_1))\| \le \lambda_2(\gamma)$$

by the definition (67). The derivation of (68) is complete upon observing that

$$\Im(B_\gamma^*(x - x_0)) = \mathcal{B}_\gamma^\top G(-i(x - x_0)).$$

□

5.2 Local Convergence

We state the local convergence theorem for arbitrary isometric A^*, not necessarily given by the Fourier measurement.

Theorem 5.7 (PAP) *For any isometric A^*, let $b = |A^* x_0|$ and $\mathcal{F}$ be given by (35). Suppose $\lambda_2 < 1$ where λ_2 is given by (66).*

For any given $0 < \epsilon < 1 - \lambda_2^2$, if $x^{(1)}$ is sufficiently close to x_0 then with probability one the AP iterates $x^{(k+1)} = \mathcal{F}^k(x^{(1)})$ converge to x_0 geometrically after global phase adjustment, i.e.

$$\left\|\alpha^{(k+1)}x^{(k+1)} - x_0\right\| \le (\lambda_2^2 + \epsilon)\left\|\alpha^{(k)}x^{(k)} - x_0\right\|, \quad \forall k \tag{71}$$

where $\alpha^{(k)} := \arg\min_\alpha\{\left\|\alpha x^{(k)} - x_0\right\| : |\alpha| = 1\}$.

Proof By Proposition 3.1 and the projected gradient formulation (34), we have $\mathcal{F}(x) = x - \nabla F(x)$.

From the definition of $\alpha^{(k+1)}$, we have

$$\begin{aligned}\left\|\alpha^{(k+1)}x^{(k+1)} - x_0\right\| &\le \left\|\alpha^{(k)}x^{(k+1)} - x_0\right\| \\ &\le \left\|\alpha^{(k)}x^{(k)} - \nabla F(\alpha^{(k)}x^{(k)}) - x_0 + \nabla F(x_0)\right\| \end{aligned} \tag{72}$$

Let $g(x) = x - \nabla F(x)$ and $\gamma(t) = x_0 + t(x - x_0)$. By the mean value theorem,

$$g(x) - g(x_0) = \int_0^1 \left[I - \nabla^2 F(\gamma(t))\right](x - x_0)dt \tag{73}$$

and hence with $x = \alpha^{(k)}x^{(k)}$ the right hand side of (72) equals

$$\begin{aligned}&\left\|\int_0^1 (I - \nabla^2 F(\gamma(t)))(\alpha^{(k)}x^{(k)} - x_0)dt\right\| \\ &\qquad = \left\|\int_0^1 \mathcal{B}_{\gamma(t)}(\rho_{\gamma(t)} \odot \mathcal{B}_{\gamma(t)}^{\top} G(-i(\alpha^{(k)}x^{(k)} - x_0)))dt\right\|\end{aligned}$$

by (60), and is bounded by

$$\begin{aligned}&\left\|\int_0^1 \mathcal{B}_{\gamma(t)}\Big((\rho_{\gamma(t)} - \mathbf{1}_J) \odot \mathcal{B}_{\gamma(t)}^{\top} G(-i(\alpha^{(k)}x^{(k)} - x_0))\Big)dt\right\| \\ &+ \left\|\int_0^1 \mathcal{B}_{\gamma(t)}\left(\mathbf{1}_J \odot \mathcal{B}_{\gamma(t)}^{\top} G(-i(\alpha^{(k)}x^{(k)} - x_0))\right)dt\right\|\end{aligned} \tag{74}$$

where $\mathbf{1}_J$ is the indicator of $J = \{j : b[j] > 0\}$.

Since $\alpha^{(k)}$ is chosen to minimize

$$\left\|\alpha^{(k)}x^{(k)} - x_0\right\|^2 = \left\|x^{(k)}\right\|^2 + \|x_0\|^2 - 2\langle\alpha^{(k)}x^{(k)}, x_0\rangle,$$

we have

$$x_0^*(\alpha^{(k)}x^{(k)}) > 0, \quad \forall k. \tag{75}$$

First we claim that for any given $\epsilon > 0$ and sufficiently small $\|\alpha^{(k)}x^{(k)} - x_0\|$ we have

$$\left\|\mathcal{B}_{\gamma(t)}\left(\mathbf{1}_J \odot \mathcal{B}_{\gamma(t)}^{\top} G\big(-i\big(\alpha^{(k)}x^{(k)} - x_0\big)\big)\right)\right\| \le (\lambda_2^2 + \epsilon/2)\left\|\alpha^{(k)}x^{(k)} - x_0\right\|. \tag{76}$$

We postpone the proof of the claim till the end.

By the above claim we bound (74) by

$$\left(\sup_{t\in(0,1)} \|\rho_{\gamma(t)} - \mathbf{1}_J\|_\infty + \lambda_2^2 + \epsilon/2\right)\left\|\alpha^{(k)}x^{(k)} - x_0\right\|.$$

For any $\epsilon > 0$, if $x^{(1)}$ is sufficiently close to x_0, then by continuity

$$\sup_{t\in(0,1)} \|\rho_{\gamma(t)} - \mathbf{1}_J\|_\infty \le \epsilon/2, \tag{77}$$

and we have from above estimate

$$\left\|\alpha^{(2)}x^{(2)} - x_0\right\| \le (\lambda_2^2 + \epsilon)\left\|\alpha^{(1)}x^{(1)} - x_0\right\|.$$

By induction and the assumption that $\lambda_2^2 + \epsilon < 1$, we have

$$\left\|\alpha^{(k+1)}x^{(k+1)} - x_0\right\| \le (\lambda_2^2 + \epsilon)\left\|\alpha^{(k)}x^{(k)} - x_0\right\|$$

from which (71) follows.

Now let us prove the above claim.

Let $\xi_1(t)$ and $\eta_1(t)$ be the leading singular (unit) vectors for $\mathcal{B}_{\gamma(t)}^\top$ and $\mathcal{B}_{\gamma(t)}$, respectively. As in Proposition 5.2, we have

$$\xi_1(t) = \frac{G(\gamma(t))}{\|G(\gamma(t))\|}, \quad \eta_1(t) = \frac{|A^*\gamma(t)|}{\|A^*\gamma(t)\|}.$$

The the continuous dependence of $\xi_1(t)$ and $\eta_1(t)$ on $\alpha^{(k)}x^{(k)}$ implies that for any $\delta > 0$

$$\sup_{t\in[0,1]} \|\xi_1(t) - \xi_1(0)\| < \delta_1, \quad \sup_{t\in[0,1]} \|\eta_1(t) - \eta_1(0)\| < \delta_1 \tag{78}$$

if $\|\alpha^{(k)}x^{(k)} - x_0\|$ is sufficiently small. Likewise, for any given $\delta_2 > 0$,

$$\sup_{t\in[0,1]} \left|\frac{\lambda_2^2(t)}{\lambda_2^2(0)} - 1\right| < \delta_2. \tag{79}$$

We note that $\lambda_2(0) > 0$ since $\mathcal{B}_{x_0}$ is full-rank.

By (75)

$$\left\langle \alpha^{(k)}x^{(k)}, i x_0\right\rangle = \left\langle x_0, i\alpha^{(k)}x^{(k)}\right\rangle = 0 \tag{80}$$

and hence

$$\begin{aligned}\left\langle \gamma(t), -i(\alpha^{(k)}x^{(k)} - x_0)\right\rangle &= t\left\langle \alpha^{(k)}x^{(k)}, -i(\alpha^{(k)}x^{(k)} - x_0)\right\rangle \\ &\quad + (1-t)\left\langle x_0, -i(\alpha^{(k)}x^{(k)} - x_0)\right\rangle = 0.\end{aligned}$$

So the following quantity

$$w := \frac{G(-i(\alpha^{(k)}x^{(k)} - x_0))}{\|G(-i(\alpha^{(k)}x^{(k)} - x_0))\|}.$$

is orthogonal to $\xi_1(t)$. By (68), $\|\mathcal{B}^\top_{\gamma(t)} w\| \le \lambda_2(t)$ so we can write

$$\mathbf{1}_J \odot \mathcal{B}^\top_{\gamma(t)} w = (c_1\eta_1(t) + c_2\eta_\perp(t))\lambda_2(t)$$

for some constants $c_1, c_2 \in \mathbb{R}, c_1^2 + c_2^2 \le 1$, and some unit vector $\eta_\perp(t) \in \mathbb{R}^N$ orthogonal to $\eta_1(t)$. Indeed,

$$c_1\lambda_2(t) = \left\langle \mathbf{1}_J \odot \eta_1(t), \mathcal{B}^\top_{\gamma(t)} w \right\rangle. \tag{81}$$

On the other hand, by the orthogonality between $\xi_1(t)$ and w,

$$\left\langle \eta_1(t), \mathcal{B}^\top_{\gamma(t)} w \right\rangle = \langle \mathcal{B}_{\gamma(t)}\eta_1(t), w\rangle = \langle \xi_1(t), w\rangle = 0. \tag{82}$$

Moreover, for any $t \in [0, 1]$,

$$\begin{aligned} \|\mathbf{1}_J \odot \eta_1(t) - \eta_1(t)\| &\le \|\mathbf{1}_J \odot \eta_1(t) - \eta(0)\| + \|\eta_1(t) - \eta_1(0)\| \\ &\le \|\eta_1(t) - \eta(0)\| + \|\eta_1(t) - \eta_1(0)\| \\ &\le 2\|\eta_1(t) - \eta_1(0)\| \end{aligned}$$

and hence by (78)

$$\sup_{t\in[0,1]} \|\mathbf{1}_J \odot \eta_1(t) - \eta_1(t)\|_2 < 2\delta_1. \tag{83}$$

The estimates (81), (82) and (83) imply

$$|c_1| \le 2\delta_1/\lambda_2(0). \tag{84}$$

Finally, combining (84) and (79), we obtain

$$\begin{aligned} \left\| \mathcal{B}_{\gamma(t)} \left(\mathbf{1}_J \odot \mathcal{B}^\top_{\gamma(t)} w \right) \right\| &= \|\mathcal{B}_{\gamma(t)}(c_1\eta_1(t) + c_2\eta_\perp(t))\|\lambda_2(t) \\ &= \lambda_2(t)\sqrt{c_1^2 + c_2^2\|\mathcal{B}_{\gamma(t)}\eta_\perp(t)\|^2} \\ &\le \lambda_2(t)\sqrt{c_1^2 + c_2^2\lambda_2^2(t)} \\ &\le \lambda_2^2(0) + \epsilon/2 \end{aligned} \tag{85}$$

by choosing δ_1, δ_2 properly. The proof of the claim is complete. □

6 Real-Constrained AP

In the case of $x_0, x \in \mathbb{R}^n$ (or $\mathbb{R}^n_+$), we adopt the new definition

$$\tilde{\lambda}_2 := \max\{\|\Im(B^*)u\| : u \in \mathbb{R}^n, \|u\| = 1\} = \|\Im(B^*)\| \tag{86}$$

which differs from the definition (67) of λ_2 in that u has all real components and hence the condition $\langle u, ix_0\rangle = 0$ is always satisfied. Since the test function u is more restricted in (86) we have $\tilde{\lambda}_2 \le \lambda_2$ defined in (66) in the one-pattern case. The spectral gap property $\lambda_2 < 1$ holds even with just one coded diffraction pattern for any complex object.

Proposition 6.1 [18] *Let $x_0 \in \mathbb{C}^n$ be not a line object. For A^* given by (5) with independently and continuously distributed mask phases,*

$$\lambda_2 = \max\{\|\Im[B^*u]\| : u \in \mathbb{C}^n, iu \perp x_0, \|u\| = 1\} < 1$$

and hence $\tilde{\lambda}_2 < 1$ with probability one.

Following *verbatim* the proof of Proposition 5.6, we have the similar result.

Proposition 6.2 *Let $x_0, x \in \mathbb{R}^n$ (or $\mathbb{R}^n_+$) with $x_0^*, x > 0$. Let γ be a convex combination of x and x_0. Then*

$$\|\Im(B_\gamma^*(x - x_0))\| \le \tilde{\lambda}_2(\gamma)\|x - x_0\| \tag{87}$$

where

$$\tilde{\lambda}_2(\gamma) := \max\{\|\Im(B_\gamma^*)u\| : u \in \mathbb{R}^n, \|u\| = 1\}.$$

The following convergence theorem is analogous to Theorem 5.7.

Theorem 6.3 (RAP) *For any isometric A^*, let $b = |A^*x_0|$ and $\mathcal{F}$ be given by (36). Suppose $\tilde{\lambda}_2 < 1$ where $\tilde{\lambda}_2$ is given by (86).*

For any given $0 < \epsilon < 1 - \tilde{\lambda}_2^2$, if $x^{(1)}$ is sufficiently close to x_0 then with probability one the AP iterates $x^{(k+1)} = \mathcal{F}^k(x^{(1)})$ converge to x_0 geometrically after global phase adjustment, i.e.

$$\left\|\alpha^{(k+1)}x^{(k+1)} - x_0\right\| \le (\tilde{\lambda}_2^2 + \epsilon)\left\|\alpha^{(k)}x^{(k)} - x_0\right\|, \quad \forall k \tag{88}$$

where $\alpha^{(k)} := x^{(k)*}x_0/|x^{(k)*}x_0|$ and $\alpha^{(k)} = 1$ if $x_0 \in \mathbb{R}^n_+$.

Proof From the definition of $\alpha^{(k+1)}$, we have

$$\left\|\alpha^{(k+1)}x^{(k+1)} - x_0\right\| \le \left\|\alpha^{(k)}x^{(k+1)} - x_0\right\| \tag{89}$$

Recalling (34), we write

$$x^{(k+1)} = \left[x^{(k)} - \nabla F\left(x^{(k)}\right)\right]_{\mathcal{X}}.$$

By the properties of linear projection,

$$\alpha^{(k)}x^{(k+1)} = \left[\alpha^{(k)}x^{(k)} - \nabla F\left(\alpha^{(k)}x^{(k)}\right)\right]_{\mathcal{X}} \tag{90}$$

and hence the right hand side of (89) equals

$$\begin{aligned}&\left\|\left[\alpha^{(k)}x^{(k)}-\nabla F(\alpha^{(k)}x^{(k)})\right]_{\mathcal{X}}-\left[x_0-\nabla F(x_0)\right]_{\mathcal{X}}\right\|\\&\qquad\le\left\|\alpha^{(k)}x^{(k)}-\nabla F\left(\alpha^{(k)}x^{(k)}\right)-x_0+\nabla F(x_0)\right\|.\end{aligned}\tag{91}$$

The rest of the proof follows *verbatim* that of Theorem 5.7 from (73) onward, except with λ_2 replaced by $\tilde{\lambda}_2$. □

7 Serial AP

To build on the theory of PAP, we assume, as for two coded diffraction patterns, $A=\left[\frac{1}{\sqrt{2}}A_1,\frac{1}{\sqrt{2}}A_2\right]$ where $A_l^*\in\mathbb{C}^{N/2\times n}$ are isometric and let $b_l=|A_l^*x_0|\in\mathbb{R}^{N/2}$.

By applying Theorem 5.7 separately to $\mathcal{F}_1$ and $\mathcal{F}_2$, we get the following bound

$$\left\|\alpha^{(k+1)}x^{(k+1)}-x_0\right\|\le\left(\left(\lambda_2^{(2)}\lambda_2^{(1)}\right)^2+\epsilon\right)\left\|\alpha^{(k)}x^{(k)}-x_0\right\|,\quad\forall k,\tag{92}$$

where

$$\lambda_2^{(l)}=\max\{\|\Im[B_l^*u]\|:u\in\mathbb{C}^n,iu\perp x_0,\|u\|=1\},\quad B_l=A_l\mathrm{diag}\left\{\frac{A_l^*x_0}{|A_l^*x_0|}\right\},$$

$l=1,2$.

But we can do better. By the projected gradient formulation (34), we have $\mathcal{F}_l(x)=x-\nabla F_l(x)$, $l=1,2$. Let $d\mathcal{F}_l$ be the Jacobian matrix of $\mathcal{F}_l$. Similar to the calculation in Proposition 5.1, we have

$$\begin{aligned}G(d\mathcal{F}_l\xi)&=G(iB_l\Im(B_l^*\xi))\\&=\begin{bmatrix}-\Im(B_l)\\\Re(B_l)\end{bmatrix}\mathcal{B}_l^\top G(-i\xi),\quad\forall\xi\in\mathbb{C}^n.\end{aligned}$$

Equivalently, we have

$$G(-id\mathcal{F}_l\xi)=\mathcal{B}_l\mathcal{B}_l^{\mathrm{T}}G(-i\xi),\quad\forall\xi\in\mathbb{C}^n.$$

Hence, by the isomorphism $\mathbb{C}^n\cong\mathbb{R}^{2n}$ via $G(-i\xi)$, we can represent the action of $d\mathcal{F}_l$ on $\mathbb{R}^{2n}$ by the real matrix

$$\mathcal{B}_l\mathcal{B}_l^\top=\begin{bmatrix}\Re(B_l)\\\Im(B_l)\end{bmatrix}\left[\Re(B_l^\top)\ \Im(B_l^\top)\right]\tag{93}$$

and the Jacobian matrix of $\mathcal{F}_2\mathcal{F}_1$ by

$$\mathcal{D}:=\mathcal{B}_2\mathcal{B}_2^\top\mathcal{B}_1\mathcal{B}_1^\top\tag{94}$$

which is the product of the Jacobian matrices of $\mathcal{F}_2$ and $\mathcal{F}_1$. Define

$$\|\mathcal{D}\|_\perp := \max\{\|\mathcal{D}\xi\| : \xi \in \mathbb{R}^{2n}, \xi \perp \xi_1, \|\xi\| = 1\}. \tag{95}$$

We have the following bound.

Proposition 7.1

$$\|\mathcal{D}\|_\perp \le \left(\lambda_2^{(2)}\lambda_2^{(1)}\right)^2.$$

Remark 7.2 By Proposition 6.1, $\lambda_2^{(l)} < 1, l = 1, 2$, and hence $\|\mathcal{D}\|_\perp < 1$.

Proof Since $\xi_1 = G(x_0)$ is the fixed point for both $\mathcal{B}_1\mathcal{B}_1^\top$ and $\mathcal{B}_2\mathcal{B}_2^\top$, the set $\{\xi \in \mathbb{R}^{2n} : \xi \perp \xi_1\}$ is invariant under both. Hence, by the calculation

$$\begin{aligned}\left\|\mathcal{B}_2\mathcal{B}_2^\top\mathcal{B}_1\mathcal{B}_1^\top\xi\right\| &= \left\|\mathcal{B}_2\mathcal{B}_2^\top\xi'\right\|, \quad \xi' = \mathcal{B}_1\mathcal{B}_1^\top\xi \\ &\le \left(\lambda_2^{(2)}\right)^2\|\xi'\| \\ &\le \left(\lambda_2^{(2)}\right)^2\left(\lambda_2^{(1)}\right)^2\|\xi\|\end{aligned}$$

the proof is complete. □

We now prove the local convergence of SAP.

Theorem 7.3 (SAP) *Let* $A = \left[\frac{1}{\sqrt{2}}A_1, \frac{1}{\sqrt{2}}A_2\right]$ *with isometric* A_1^* *and* A_2^*, $b = |A^*x_0|$ *and* $\mathcal{F}$ *be given by* (39). *Suppose* $\|\mathcal{D}\|_\perp < 1$ *where* $\|\mathcal{D}\|_\perp$ *is given by* (95).

For any given $0 < \epsilon < 1 - \|\mathcal{D}\|_\perp$, *if* $x^{(1)}$ *is sufficiently close to* x_0 *then with probability one the AP iterates* $x^{(k+1)} = \mathcal{F}^k(x^{(1)})$ *converge to* x_0 *geometrically after global phase adjustment, i.e.*

$$\left\|\alpha^{(k+1)}x^{(k+1)} - x_0\right\| \le (\|\mathcal{D}\|_\perp + \epsilon)\left\|\alpha^{(k)}x^{(k)} - x_0\right\|, \quad \forall k \tag{96}$$

where $\alpha^{(k)} := \arg\min_\alpha\{\|\alpha x^{(k)} - x_0\| : |\alpha| = 1\}$.

Proof At the optimal phase $\alpha^{(k)}$ adjustment for $x^{(k)}$, we have

$$\Im(x_0^*\alpha^{(k)}x^{(k)}) = 0$$

and hence

$$\left\langle\alpha^{(k)}x^{(k)} - x_0, ix_0\right\rangle = \left\langle\alpha^{(k)}x^{(k)}, ix_0\right\rangle = \Re\left(\left(\alpha^{(k)}x^{(k)}\right)^* ix_0\right) = 0 \tag{97}$$

which implies that

$$w^{(k)} := -i\left(\alpha^{(k)}x^{(k)} - x_0\right)$$

is orthogonal to the leading right singular vector $\xi_1 = G(x_0)$ of $\mathcal{B}_l^*$, $l = 1, 2$:

$$\xi_1 \perp G(w^{(k)}), \quad \forall k \tag{98}$$

cf. Proposition 5.2.

We have for $k = 1, 2, 3, \ldots$

$$\begin{aligned} \left\|\alpha^{(k+1)}\mathcal{F}_2\mathcal{F}_1(x^{(k)}) - x_0\right\| &\le \left\|\alpha^{(k)}\mathcal{F}_2\mathcal{F}_1(x^{(k)}) - x_0\right\| \\ &= \left\|\mathcal{F}_2\mathcal{F}_1(\alpha^{(k)}x^{(k)}) - \mathcal{F}_2\mathcal{F}_1(x_0)\right\| \\ &= \left\|\mathcal{D}G(w^{(k)})\right\| + o(\left\|w^{(k)}\right\|) \\ &\le \max_{\substack{\xi\perp\xi_1 \\ \|\xi\|=1}} \|\mathcal{D}\xi\|\left\|w^{(k)}\right\| + o(\left\|w^{(k)}\right\|), \end{aligned}$$

where $\mathcal{D}$ defined in (94) is the Jacobian matrix of $\mathcal{F}_2\mathcal{F}_1$, and hence

$$\left\|w^{(k+1)}\right\| \le \|\mathcal{D}\|_{\perp}\left\|w^{(k)}\right\| + o\big(\left\|w^{(k)}\right\|\big). \tag{99}$$

By induction on k with $w^{(1)}$ sufficiently small, we have the desired result (96). □

8 Numerical Experiments

8.1 Test Images

Let C, B and P denote the 256×256 non-negatively valued Cameraman, Barbara and Phantom images, respectively (Fig. 1).

For one-pattern simulation, we use C and P for test images. For the two-pattern simulations, we use the complex-valued images, Randomly Signed Cameraman–Barbara (RSCB) and Randomly Phased Phantom (RPP), constructed as follows.

(a) **(b)** **(c)**

Fig. 1 Test images: **a** Cameraman, **b** Barbara, **c** Phantom

RSCB Let $\{\beta_R(\mathbf{n}) = \pm 1\}$ and $\{\beta_I(\mathbf{n}) = \pm 1\}$ be i.i.d. Bernoulli random variables. Let

$$x_0 = \beta_R \odot C + i\beta_I \odot B.$$

RPP Let $\{\phi(\mathbf{n})\}$ be i.i.d. uniform random variables over $[0, 2\pi]$ and let

$$x_0 = P \odot e^{i\phi}.$$

We use the relative error (RE)

$$\mathrm{RE} = \min_{\theta\in[0,2\pi)} \|x_0 - e^{i\theta}x\|/\|x_0\|$$

as the figure of merit and the relative residual (RR)

$$\mathrm{RR} = \|b - |A^*x|\|/\|x_0\|$$

as a metric for setting the stopping rule.

8.2 Wirtinger Flow

WF is a two-stage algorithm proposed by [13] and further improved by [11] (the truncated version).

The first stage is the spectral initialization (Algorithm 2). For the truncated spectral initialization (15), the parameter τ can be optimized by tracking and minimizing the residual $\|b - |A^*x_k|\|$.

The second stage is a gradient descent method for the cost function

$$F_{\mathrm{w}}(x) = \frac{N}{2}\||A^*x|^2 - b^2\|^2 \tag{100}$$

where a proper normalization is introduced to adjust for notational difference and facilitate a direct comparison between the present set-up (A^* is an isometry) and that of [13]. A motivation for using (100) instead of (21) is its global differentiability.

Below we evaluate these two stages separately and use the notation WF to denote primarily the second stage defined by the WF map

$$\begin{aligned}\mathcal{F}_{\mathrm{w}}(x^{(k)}) &= x^{(k)} - \frac{s^{(k)}}{\|x^{(1)}\|^2}\nabla F_{\mathrm{w}}(x^{(k)}) \\ &= x^{(k)} - \frac{s^{(k)}}{\|x^{(1)}\|^2} A\left(N\left(|A^*x^{(k)}|^2 - |b|^2\right) \odot A^*x^{(k)}\right),\end{aligned} \tag{101}$$

for $k = 1, 2, \ldots,$ with $s^{(k)}$ is the step size at the k-th iteration. Each step of WF involves twice FFT and once pixel-wise operations, comparable to the computational complexity of one iteration of PAP.

In [13] (Theorem 5.1), a basin of attraction at x_0 of radius $O(n^{-1/2})$ is established for WF for a sufficiently small constant $s^{(k)} = s$. No explicit bound on s is available. A disadvantage of WF is that the iterates diverge if the stepsize is too large (see Sect. 8.6 for more details).

For comparison, consider the projected gradient formulation of PAP

$$\begin{aligned} \mathcal{F}(x^{(k)}) &= x^{(k)} - \nabla F(x^{(k)}) \\ &= x^{(k)} - A\left(\left(\mathbf{1} - \frac{b}{|A^*x^{(k)}|}\right) \odot A^*x^{(k)}\right) \end{aligned} \tag{102}$$

which is well-defined if $\operatorname{supp}(b) \subseteq \operatorname{supp}(A^*x)$. Eq. (102) implies a constant step size 1.

In addition, it may be worthwhile to compare the "weights" in ∇F_{w} and ∇F:

$$N\left(|A^*x^{(k)}|^2 - |b|^2\right) = N|A^*x^{(k)}|^2\left(\mathbf{1} - \frac{|b|^2}{|A^*x^{(k)}|^2}\right) \quad \text{in } \nabla F_{\mathrm{w}} \tag{103}$$

versus

$$\mathbf{1} - \frac{b}{|A^*x^{(k)}|} \quad \text{in } \nabla F. \tag{104}$$

Notice that the factor $N|A^*x^{(k)}|^2$ in (103) is approximately Nb^2 if $x^{(k)} \approx x_0$. Like the truncated spectral initialization, the truncated Wirtinger flow seeks to reduce the variability of the weights in (103) by introducing 3 new control parameters [11].

8.3 One-Pattern Experiments

Figure 2 shows that the null initialization x_{null} is more accurate than the spectral vector x_{spec} and the truncated spectral vector $x_{\text{t-spec}}$ in approximating the true images. For the Cameraman (resp. the Phantom) $\mathrm{RR}(x_{\mathrm{null}})$ can be minimized by setting $\gamma \approx 0.70$ (resp. $\gamma \approx 0.74$). The optimal parameter τ^2 for $x_{\text{t-spec}}$ in (15) is about 4.1 (resp. 4.6).

Next we compare the performances of PAP and WF [13] with x_{null} as well as the random initialization x_{rand}. Each pixel of x_{rand} is independently sampled from the uniform distribution over $[0, 1]$.

To account for the real/positivity constraint, we modify (101) as

$$\mathcal{F}_{\mathrm{w}}(x^{(k)}) = \left[x^{(k)} - \frac{s^{(k)}}{\|x^{(1)}\|^2}\nabla F_{\mathrm{w}}(x^{(k)})\right]_{\mathcal{X}}, \quad \mathcal{X} = \mathbb{R}^n,\ \mathbb{R}^n_+. \tag{105}$$

As shown in Fig. 3, the convergence of both PAP and WF is faster with x_{null} than x_{rand}. In all cases, PAP outperforms WF.

Also, the median value $\gamma = 0.5$ for initialization is as good as the optimal value. The convergence of PAP with random initial condition x_{rand} suggests *global* convergence to the true object in the one-pattern case with the positivity constraint.

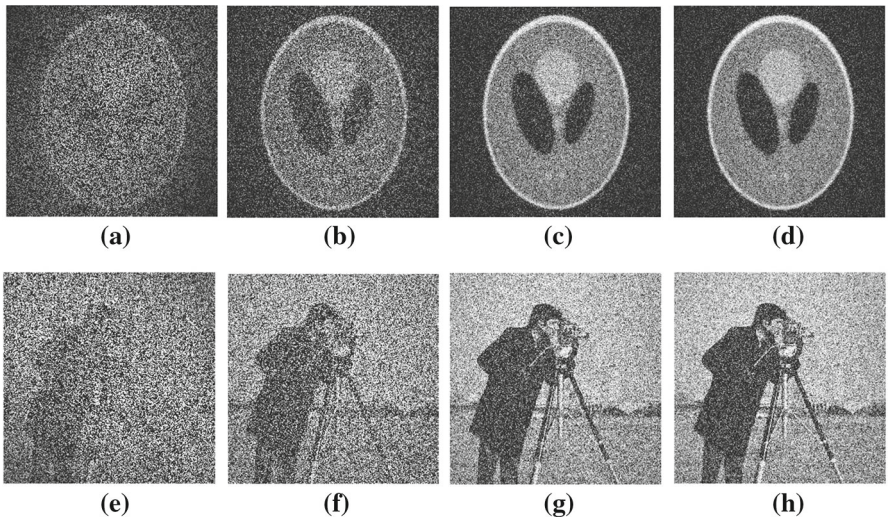

Fig. 2 Initialization with one pattern of the Phantom (**a** RE(x_{spec}) $= 0.9604$, **b** RE($x_{\text{t-spec}}$) $= 0.7646$, **c** RE(x_{null}) $= 0.5119$, **d** RE(x_{null}) $= 0.4592$) and the Cameraman (**e** RE(x_{spec}) $= 0.8503$, **f** RE($x_{\text{t-spec}}$) $= 0.7118$, **g** RE(x_{null}) $= 0.4820$, (h) RE(x_{null}) $= 0.4423$)

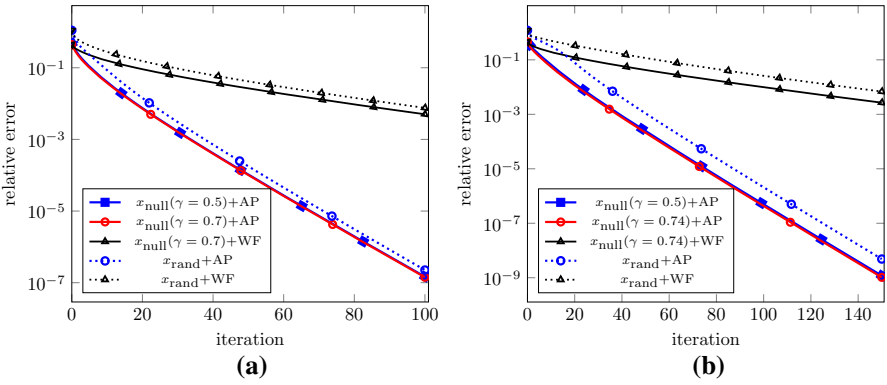

Fig. 3 Semi-log plot of RE versus iteration in the one-pattern case with the **a** Cameraman and **b** Phantom. WF is tested with the optimized step size $s = 0.2$

8.4 Two-Pattern Experiments

We use the complex images, RSCB and RPP, for the two -pattern simulations.

Figure 4 shows that x_{null} is more accurate than the x_{spec} and $x_{\text{t-spec}}$ in approximating x_0. The difference in RE between the initializations with the median value and the optimal values is less than 3%.

Figure 5 shows that for the two-pattern case PAP outperforms WF, both with the null initialization.

As Fig. 6 shows, SAP converges much faster than PAP and takes about half the number of iterations to converge to the object. Different samples correspond to different

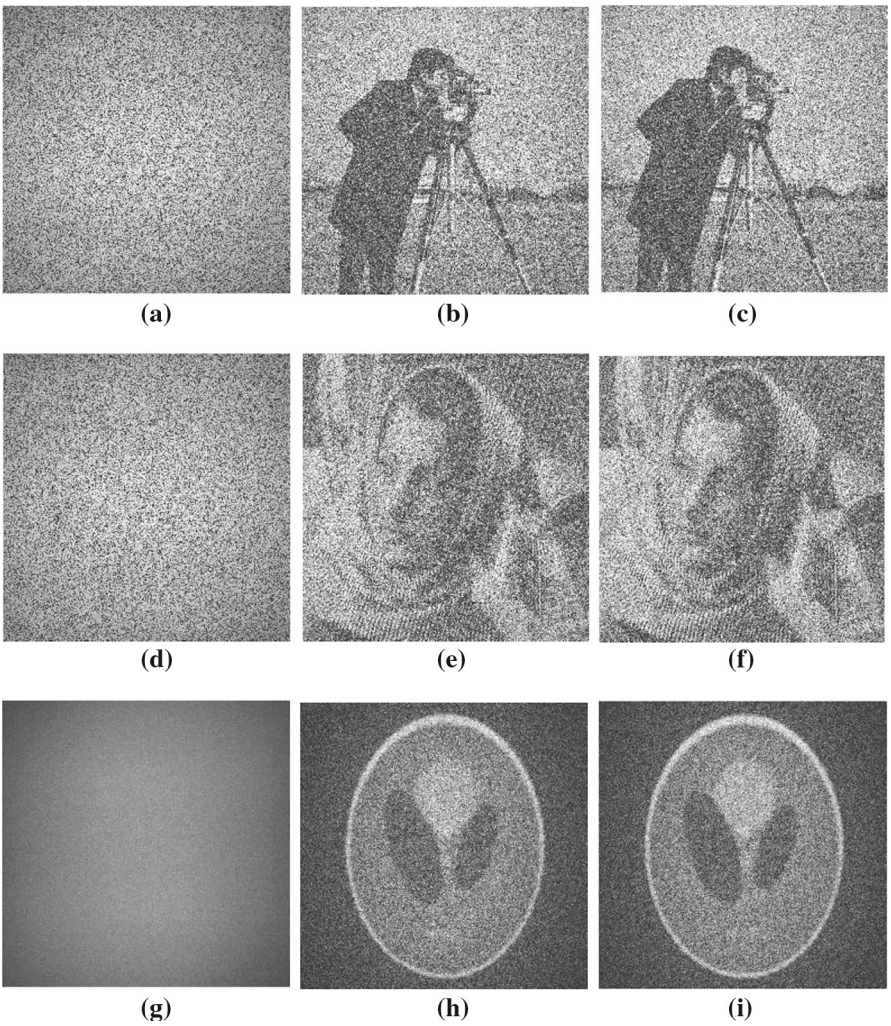

Fig. 4 Initialization with two patterns for RSCB (**a**, **d**) RE($x_{\text{t-spec}}$) = 1.3954, (**b**, **e**) RE(x_{null}) = 0.5736, (**c**, **f**) RE(x_{null}) = 0.5416) and RPP (**g**)RE($x_{\text{t-spec}}$) = 1.3978, (**h**) RE(x_{null}) = 0.7399, (**i**) RE(x_{null}) = 0.7153)

realizations of random masks, showing robustness with respect to the ensemble of random masks. SAP with the null initialization also outperforms the Fourier-domain Douglas–Rachford algorithm [18].

Figure 7 shows the semi-log plot of RE versus iteration for the (a) one-pattern and (b) two-pattern cases. The dotted lines represent the geometric series $\{\tilde{\lambda}_2^{2k}\}_{k=1}^{200}$, $\{\lambda_2^{2k}\}_{k=1}^{200}$ and $\|\mathcal{D}\|_{\perp}^{k}$ (the pink line in (a) and the red and the blue lines in (b)), which track well the actual iterates (the black-solid curve in (a) and the blue- and the red-solid curves in (b)), consistent with the predictions of Theorems 5.7, 6.3 and 7.3. In particular, SAP has a better rate of convergence than PAP (0.7946 vs 0.9086).

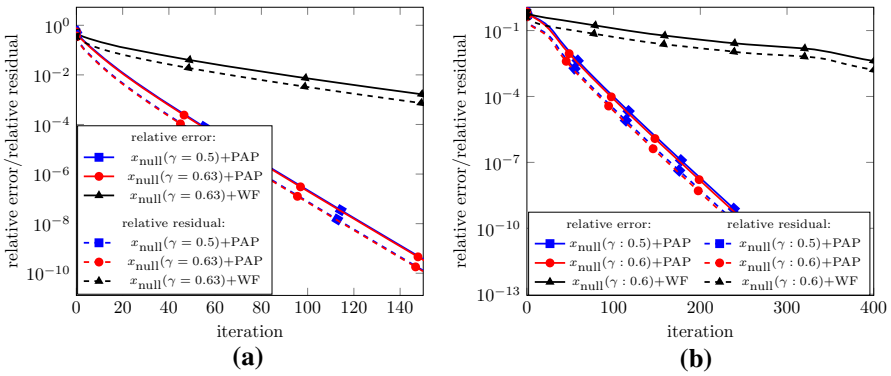

Fig. 5 Semi-log plot of RE and RR versus iteration for PAP and WF with two patterns. WF is tested with the optimized step size **a** $s = 0.2$ and **b** $s = 0.15$

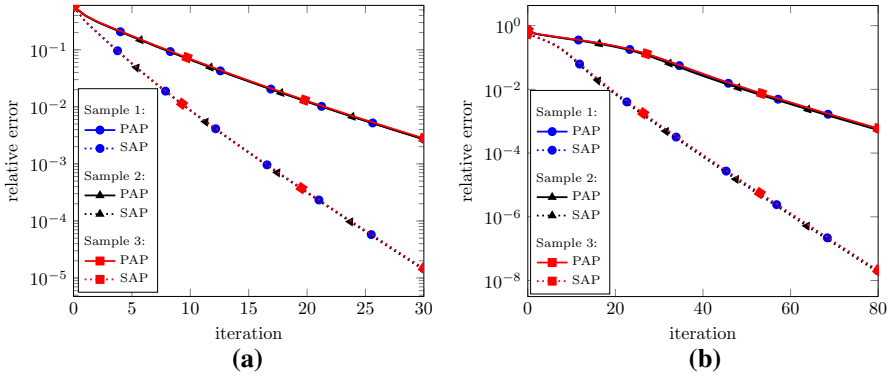

Fig. 6 Semi-log plot of RE versus iteration of PAP and SAP in the two-pattern case ($\gamma = 0.5$)

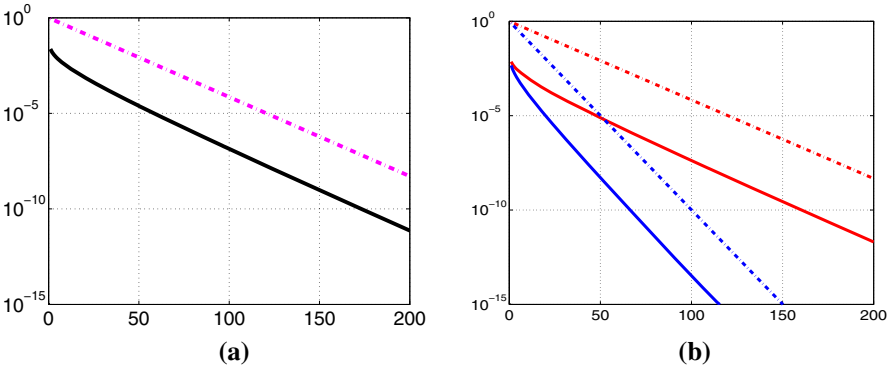

Fig. 7 RE on the log scale versus iteration with **a** one pattern and **b** two patterns (PAP in *red*, SAP in *blue*). The *solid curves* are the AP iterates and the *dotted lines* are the geometric series predicted by the theory (Color figure online)

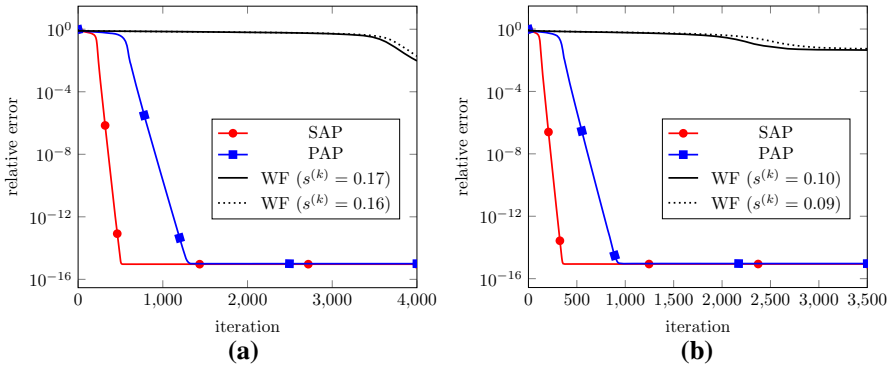

Fig. 8 Semi-log plot of RE versus iteration of SAP, PAP and WF with two patterns and the null initialization ($\gamma = 0.38$ and 0.4 for RSCB and RPP, respectively)

8.5 Oversampling Ratio

Phase retrieval with just one coded diffraction pattern without the real/positivity constraint has many solutions [28] and as a result AP with the null initialization does not perform well numerically.

A natural question then is, Would happen if we measure two coded diffraction patterns each with fewer samples?

The amount of data in each coded diffraction pattern is measured by the oversampling ratio

$$\rho = \frac{\text{Number of data in } \textbf{each} \text{ coded diffraction pattern}}{\text{Number of image pixels}},$$

which is approximately 4 in the standard oversampling.

For the two-pattern results in Fig. 8, we use $\rho = 1.65, 1.96$ (respectively for RSCB and RPP) and hence $N \approx 3.3n, 3.92n$ (respectively for RSCB and RPP). For $n = 256 \times 256$, $3.3n \approx 2.16269 \times 10^5$, $3.92n \approx 2.56901 \times 10^5$ are both significantly less than $(2\sqrt{n} - 1)^2 = 2.61121 \times 10^5$, the number of data in a coded diffraction pattern with the standard oversampling.

As expected, convergence is slowed down for both methods (much less so for SAP) as the oversampling ratio decreases. Nevertheless, both SAP and PAP converge rapidly to the true solution, reaching machine precision, within 500 and 1200 iterations, while WF fails to converge within 4000 steps for RSCB and stagnates after 3000 iterations for RPP.

8.6 Noise Stability

We test the performance of AP and WF with the Gaussian noise model where the noisy data is generated by

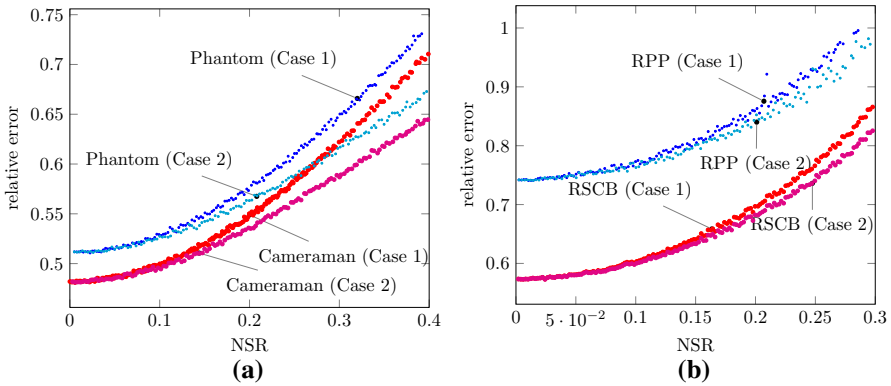

Fig. 9 RE versus NSR of the null initialization ($\gamma = 0.5$)

$$b_{\text{noisy}} = |A^* x_0 + \text{complex Gaussian noise}|.$$

The noise is measured by the Noise-to-Signal Ratio (NSR)

$$\text{NSR} = \frac{\|b_{\text{noisy}} - |A^* x_0|\|_2}{\|A^* x_0\|_2}.$$

As pointed out in Sect. 2.3, since the null initialization depends only on the choice of the index set I and does not depend explicitly on b, the method is more noise-tolerant than other initialization methods.

Let $\hat{x}_{\text{null}}$ be a *unit* leading singular vector of A_{I_c}. In order to compare the effect of normalization, we normalize a null vector in two different ways

$$\text{Case 1.} \quad x_{\text{null}} = \alpha \|b_{\text{noisy}}\| \cdot \hat{x}_{\text{dual}} \tag{106}$$

$$\text{Case 2.} \quad x_{\text{null}} = \alpha \|x_0\| \cdot \hat{x}_{\text{dual}} \tag{107}$$

and then compute their respective relative errors versus NSR. As shown in Fig. 9, the slope of *the increase in RE* versus NSR is less than 1 in all cases. Remarkably, the slope is much smaller than 1 for small NSR when the performance curves are strictly convex and independent of the way of normalization. In particular, the difference between the two cases is not noticeable until NSR > 0.1. For larger NSR, however, the proper normalization with $\|x_0\|$ (Case 2) can significantly reduce the error.

The difference between the initialization errors of RPP and RSCB would disappear by and large after the AP iteration converges, indicating the null initialization enters the basin of attraction of the noisy feasibility set for both images, see Fig. 11.

Next, we compare the performance of AP and WF with the null initialization in the noisy case. Noisy data would affect the choice of step size for WF. For example, in contrast to the noiseless case shown in Fig. 5, the WF iterates diverge, respectively, with $s = 0.2$ for RSCB at NSR = 0.3 and with $s = 0.15$ for RPP at NSR = 0.2. We choose a smaller step size $s = 0.1$ with which all subsequent WF iterations converge eventually.

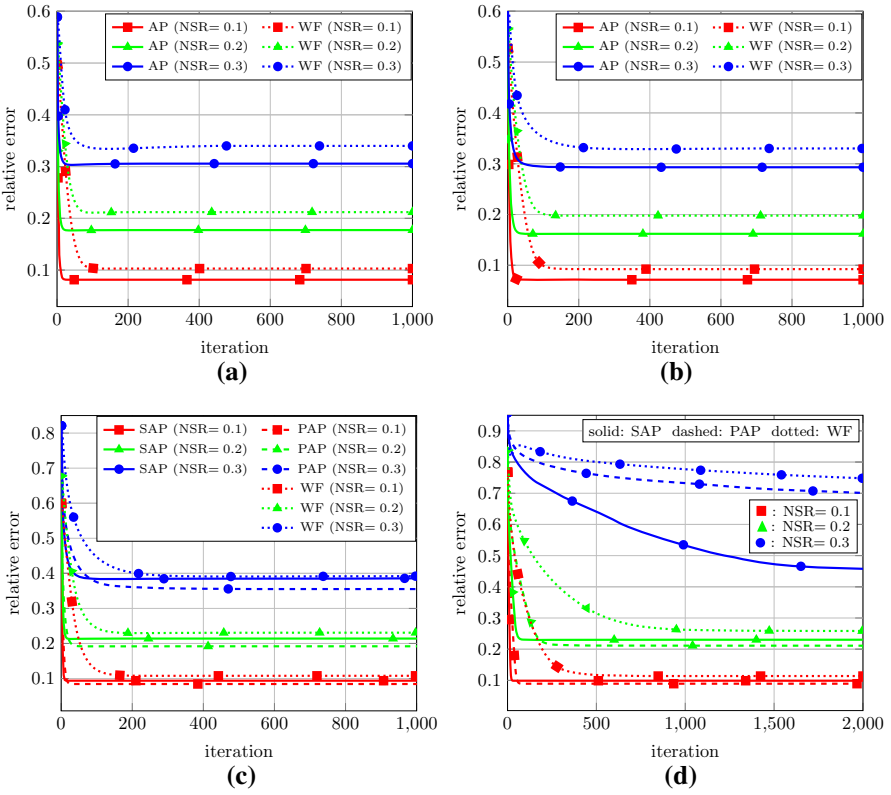

Fig. 10 Relative error versus iteration with (**a**, **b**) one and (**c**, **d**) two patterns at NSR = 0.1, 0.2, 0.3 (The step size of WF is $s = 0.1$.)

Figure 10 shows the RE versus iteration of AP and WF at NSR = 0.1, 0.2, 0.3. Convergence is achieved well within 500 iterations for both AP and WF in (a), (b) and (c). For RPP in (d), convergence is slowed down at higher NSR, especially for WF. We observe that while SAP converges the fastest but PAP achieves the lowest error except for RPP at NSR = 0.3 where PAP has not yet converged in 2000 iterations. The improved accuracy of PAP over SAP may be explained by the averaging effect in (40).

Figure 11 shows the RE of AP and WF with the null initialization with 500 iterations for the one-pattern case and 1000 iterations for the two-pattern case. In view of Fig. 10, Fig 11a, b and c exhibit fully convergent error curves while the error curves in Fig. 11(d) are fully convergent only for NSR ≤ 0.2.

Clearly, AP consistently achieves a smaller error than WF, with a noise amplification factor slightly above 1. For RPP, WF, PAP and SAP fail to converge in 1000 steps beyond 20, 25 and 28% NSR, respectively, hence the scattered data points. Increasing the maximum number of iterations can bring the upward "tails" of the curves back to roughly straight lines as in other plots.

As in Fig. 9, if $\|x_0\|$ is known explicitly, we can apply AP with the normalized noisy data

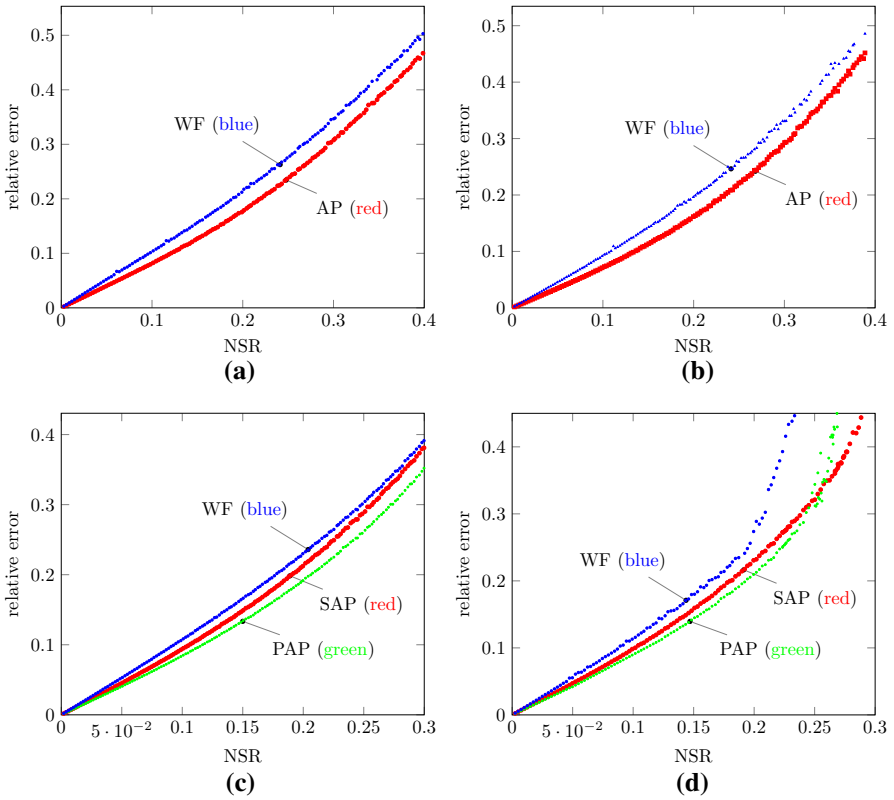

Fig. 11 RE versus NSR with one (*top row*, 500 iterations) and two (*bottom row*, 1000 iterations) patterns (The step size of WF is $s = 0.1$.)

$$\hat{b}_{\text{noisy}} = b_{\text{noisy}} \frac{\|x_0\|}{\|b_{\text{noisy}}\|}$$

and improve the performance shown in Figs. 10 and 11. And the improvement is particularly significant for larger NSR. For simplicity of presentation, the results are omitted here.

9 Conclusion and Discussion

Under the uniqueness framework of [28] (reviewed in Sect. 1.1), we have proved local geometric convergence for AP of various forms and characterized the convergence rate in terms of a spectral gap. Other literature either demands a large number of coded diffraction patterns [13,14] or asserts sublinear convergence [49]. More importantly, we have demonstrated the null initialization to be an effective initialization method with numerical performance superior to the spectral initialization and its truncated version [11,13]. In practice AP with the null initialization is a globally convergent algorithm for phase retrieval with one or two coded diffraction patterns.

Of course, a positive spectral gap does not necessarily lead to a significantly sized basin of attraction for the true object. By Remark 5.5 AP with just one coded diffraction pattern without the realness constraint still has a positive spectral gap and thus converges geometrically if the initialization is sufficiently close to the true object. However, the null initialization with one coded pattern without the realness constraint is evidently outside of the basin of attraction of AP (not shown). This is likely because the corresponding phase retrieval has many solutions and thus no initialization method can possibly succeed. On the other hand, AP with one coded diffraction pattern under the realness constraint converges globally with randomly selected initial guess (Fig. 3) because the uniqueness of solution is restored.

This observation points to the importance of the design of measurement scheme besides the choice of algorithm (e.g. AP vs WF). Results that do not take the measurement scheme into account (e.g. [41,49]) are likely to be sub-optimal in both theory and practice.

A reasonable question is, How much can the measurement scheme be relaxed from that of [28]? Fig. 8 gives a tentative answer to one aspect of the question: the number of measurement data may be reduced by as much as half and still maintains a good numerical performance. Another aspect of the question is about the type of masks to be used in measurement: indeed, besides the fine-grained (independently distributed) masks discussed in Sect. 1.1, the coarse-grained (correlated) masks can have a good numerical performance as well (see [29,30]).

A shortcoming of the present work is that we were unable to provide a useful estimate for the size of the basin of attraction for AP; our current estimate is pessimistic due to technical difficulty (not shown). Another is that we were unable to give an error bound for AP in the case of noisy data. And finally it remains an open problem to prove global convergence of our approach (AP + the null initialization).

These questions are particularly enticing in view of superior numerical performances that strongly indicate a large basin of attraction, a high degree of noise tolerance and global convergence from randomly selected initial data.

Acknowledgements Research of P. Chen is supported in part by the Grant 103-2115-M-005-006-MY2 from Ministry of Science and Technology, Taiwan, and US NIH Grant U01-HL-114494. Research of A. Fannjiang is supported in part by US National Science Foundation Grant DMS-1413373 and Simons Foundation Grant 275037.

References

1. Balan, R., Wang, Y.: Invertibility and robustness of phaseless reconstruction. Preprint: arXiv:1308.4718 (2013)
2. Balan, R., Casazza, P., Edidin, D.: On signal reconstruction without phase. Appl. Comput. Harmon. Anal. **20**, 345–356 (2006)
3. Balan, R., Bodmann, B.G., Casazza, P.G., Edidin, D.: Painless reconstruction from magnitudes of frame coefficients. J. Fourier Anal. Appl. **15**, 488–501 (2009)
4. Bandeira, A.S., Cahill, J., Mixon, D.G., Nelson, A.A.: Saving phase: Injectivity and stability for phase retrieval. Appl. Comput. Harmon. Anal. **37**, 106–125 (2014)
5. Bandeira, A.S., Chen, Y., Mixon, D.: Phase retrieval from power spectra of masked signals. Inform. Infer. (2014). Doi:10.1093/imaiai/iau002

6. Bauschke, H.H., Borwein, J.: On projection algorithms for solving convex feasibility problems. SIAM Rev. **38**, 367–426 (1996)
7. Bauschke, H.H., Combettes, P.L., Luke, D.R.: Phase retrieval, error reduction algorithm, and Fienup variants: a view from convex optimization. J. Opt. Soc. Am. A **19**, 13341–1345 (2002)
8. Bauschke, H.H., Combettes, P.L., Luke, D.R.: Finding best approximation pairs relative to two closed convex sets in Hilbert spaces. J. Approx. Theory **127**, 178–192 (2004)
9. Bertsekas, D.P.: Nonlinear Programming. Athena Scientific, Belmont (2003)
10. Bregman, L.M.: The method of successive projection for finding a common point of convex sets. Soviet Math. Dokl. **162**, 688–692 (1965)
11. Candès, E.J., Chen, Y.: Solving random quadratic systems of equations is nearly as easy as solving linear systems. arXiv:1505.05114 (2015)
12. Candès, E.J., Strohmer, T., Voroninski, V.: Phaselift: exact and stable signal recovery from magnitude measurements via convex programming. Commun. Pure Appl. Math. **66**, 1241–1274 (2013)
13. Candes, E.J., Li, X., Soltanolkotabi, M.: Phase retrieval via Wirtinger flow: theory and algorithms. IEEE Trans. Inform. Theory **61**(4), 1985–2007 (2015)
14. Candes, E.J., Li, X., Soltanolkotabi, M.: Phase retrieval from coded diffraction patterns. Appl. Comput. Harmon. Anal. **39**, 277–299 (2015)
15. Chai, A., Moscoso, M., Papanicolaou, G.: Array imaging using intensity-only measurements. Inverse Probl. **27**(1), 015005 (2011)
16. Chapman, H.N., et al.: Femtosecond X-ray protein nanocrystallography. Nature **470**, 73–77 (2011)
17. Chapman, H.N., Caleman, C., Timneanu, N.: Diffraction before destruction. Philos. Trans. R. Soc. B **369**, 20130313 (2014)
18. Chen, P., Fannjiang, A.: Phase retrieval with a single mask by Douglas–Rachford algorithms. Appl. Comput. Harmon. Anal. (2016). doi:10.1016/j.acha.2016.07.003
19. Chen, P., Fannjiang, A., Liu, G.: Phase retrieval by linear algebra. arXiv:1607.07484
20. Cheney, W., Goldstein, A.: Proximity maps for convex sets. Proc. Am. Math. Soc. **10**, 448–450 (1959)
21. Cimmino, G.: Calcolo approssimato per le soluzioni dei sistemi di equazioni lineari. Ric. Sci. Progr. Tecn. Econom. Naz. **16**, 326–333 (1938)
22. Conca, A., Edidin, D., Hering, M., Vinzant, C.: An algebraic characterization of injectivity in phase retrieval. Appl. Comput. Harmon. Anal. **38**, 346–356 (2015)
23. Davidson, K.R., Szarek, S.J.: Local operator theory, random matrices and Banach spaces. In: Lindenstrauss, J. (ed.) Handbook of the Geometry of Banach Spaces, pp. 317–366. North-Holland, Amsterdam (2001)
24. Demanet, L., Hand, P.: Stable optimizationless recovery from phaseless linear measurements. J. Fourier Anal. Appl. **20**, 199–221 (2014)
25. Deutsch, F.: Best Approximation in Inner Product Spaces. Springer, New York (2001)
26. Dobson, D.C.: Phase reconstruction via nonlinear least-squares. Inverse Probl. **8**, 541–557 (1992)
27. Eldar, Y.C., Mendelson, S.: Phase retrieval: stability and recovery guarantees. Appl. Comput. Harmon. Anal. **36**, 473–494 (2014)
28. Fannjiang, A.: Absolute uniqueness of phase retrieval with random illumination. Inverse Probl. **28**, 075008 (2012)
29. Fannjiang, A., Liao, W.: Phase retrieval with random phase illumination. J. Opt. Soc. A **29**, 1847–1859 (2012)
30. Fannjiang, A., Liao, W.: Fourier phasing with phase-uncertain mask. Inverse Probl. **29**, 125001 (2013)
31. Fienup, J.R.: Phase retrieval algorithms: a comparison. Appl. Opt. **21**, 2758–2769 (1982)
32. Fienup, J.R.: Phase retrieval algorithms: a personal tour. Appl. Opt. **52**, 45–56 (2013)
33. Gerchberg, R.W., Saxton, W.O.: A practical algorithm for the determination of the phase from image and diffraction plane pictures. Optik **35**, 237–246 (1972)
34. Goldstein, A.A.: Convex programming in Hilbert space. Bull. Am. Math. Soc. **70**, 709–710 (1964)
35. Gross, D., Krahmer, F., Kueng, R.: A partial derandomization of phaselift using spherical designs. arXiv:1310.2267 (2013)
36. Hayes, M.: The reconstruction of a multidimensional sequence from the phase or magnitude of its Fourier transform. IEEE Trans. Acoust. Speech Signal Process **30**, 140–154 (1982)
37. Kaczmarz, S.: Angenäherte Auflösung von Systemen linearer Gleichungen. Bull. Int. Acad. Pol. Sci. Lett. Ser. A **35**, 355–357 (1937)
38. Klibanov, M.K.: On the recovery of a 2-D function from the modulus of its Fourier transform. J. Math. Anal. Appl. **323**, 818–843 (2006)

39. Klibanov, M.K.: Uniqueness of two phaseless non-overdetermined inverse acoustics problems in 3-d. Appl. Anal. **93**, 1135–1149 (2013)
40. Levitin, E.S., Polyak, B.T.: Constrained minimization methods. USSR Comput. Math. Math. Phys. **6**, 1–50 (1965)
41. Lewis, A.S., Luke, D.R., Malick, J.: Local linear convergence for alternating and averaged nonconvex projections. Found. Comput. Math. **9**(4), 485–513 (2009)
42. Li, X., Voroninski, V.: Sparse signal recovery from quadratic measurements via convex programming. SIAM J. Math. Anal. **45**(5), 3019–3033 (2013)
43. Marchesini, S.: A unified evaluation of iterative projection algorithms for phase retrieval. Rev. Sci. Instrum. **78**, 011301 (2007)
44. Miao, J., Sayre, D., Chapman, H.N.: Phase retrieval from the magnitude of the Fourier transforms of nonperiodic objects. J. Opt. Soc. Am. A **15**, 1662–1669 (1998)
45. Miao, J., Kirz, J., Sayre, D.: The oversampling phasing method. Acta Crystallogr. D **56**, 1312–1315 (2000)
46. Migukin, A., Katkovnik, V., Astola, J.: Wave field reconstruction from multiple plane intensity-only data: augmented Lagrangian algorithm. J. Opt. Soc. Am. A **28**, 993–1002 (2011)
47. Netrapalli, P., Jain, P., Sanghavi, S.: Phase retrieval using alternating minimization. IEEE Trans. Signal Proc. **63**, 4814–4826 (2015)
48. Neutze, R., Wouts, R., van der Spoel, D., Weckert, E., Hajdu, J.: Potential for biomolecular imaging with femtosecond X-ray pulses. Nature **406**, 753–757 (2000)
49. Noll, D., Rondepierre, A.: On local convergence of the method of alternating projections. Found. Comput. Math. **16**, 425–455 (2016)
50. Ohlsson, H., Yang, A.Y., Dong, R., Sastry, S.S.: Compressive phase retrieval from squared output measurements via semidefinite programming. arXiv:1111.6323 (2011)
51. Ranieri, J., Chebira, A., Lu, Y.M., Vetterli, M.: Phase retrieval for sparse signals: uniqueness conditions. arXiv:1308.3058 (2013)
52. Schwarz, H.A.: Ueber einen Grenzübergang durch alternirendes Verfahren. Vierteljahrsschrift Naturforschenden Gessellschaft in Zurich **15**, 272–286 (1870)
53. Shechtman, Y., Eldar, Y.C., Cohen, O., Chapman, H.N., Jianwei, M., Segev, M.: Phase retrieval with application to optical imaging: a contemporary overview. IEEE Mag. Signal Proc. **32**(3), 87–109 (2015)
54. Seibert, M.M., et al.: Single mimivirus particles intercepted and imaged with an X-ray laser. Nature **470**, U78–U86 (2011)
55. von Neuman, J.: Functional Operators. Vol. II. The Geometry of Orthogonal Spaces. Annals of Math. Studies, vol. 22. Princeton University Press. Reprint of notes distributed in 1933 (1950)
56. Waldspurger, I.: Phase retrieval with random Gaussian sensing vectors by alternating projections. arXiv:1612.04330
57. Waldspurger, I., d'Aspremont, A., Mallat, S.: Phase recovery, maxCut and complex semidefinite programming. arXiv:1206.0102
58. Wei, K.: Solving systems of phaseless equations via Kaczmarz methods: a proof of concept study. Inverse Probl. **31**, 125008 (2015)
59. Yin, P., Xin, J.: Phaseliftoff: an accurate and stable phase retrieval method based on difference of trace and Frobenius norms. Commun. Math. Sci. **13**, 1033–1049 (2015)